

Dalton Transactions

Accepted Manuscript



This is an *Accepted Manuscript*, which has been through the Royal Society of Chemistry peer review process and has been accepted for publication.

Accepted Manuscripts are published online shortly after acceptance, before technical editing, formatting and proof reading. Using this free service, authors can make their results available to the community, in citable form, before we publish the edited article. We will replace this *Accepted Manuscript* with the edited and formatted *Advance Article* as soon as it is available.

You can find more information about *Accepted Manuscripts* in the [Information for Authors](#).

Please note that technical editing may introduce minor changes to the text and/or graphics, which may alter content. The journal's standard [Terms & Conditions](#) and the [Ethical guidelines](#) still apply. In no event shall the Royal Society of Chemistry be held responsible for any errors or omissions in this *Accepted Manuscript* or any consequences arising from the use of any information it contains.

Cite this: DOI: 10.1039/c0xx00000x

www.rsc.org/xxxxxx

ARTICLE TYPE

Reticular three-dimensional 3d–4f frameworks constructed through substituted imidazole–dicarboxylate: syntheses, luminescence and magnetic properties study

Xun Feng,^{a,*} Yu-Quan Feng,^b Jun Jing Chen^b, Seik-Weng Ng,^c Li-Ya Wang,^{b, a,*} and Jin-Zhong Guo,^a

Received (in XXX, XXX) Xth XXXXXXXXXX 20XX, Accepted Xth XXXXXXXXXX 20XX

DOI: 10.1039/b000000x

A family of heteronuclear metal organic frameworks (MOFs) using of lanthanide and transition metal ion based on a rigid ligand of substituted imidazoledicarboxylic acid, namely, $\{[\text{Ln}_2\text{Zn}_2(\mu_3\text{-Hmimda})_2(\mu_3\text{-mimda})_2\cdot 4\text{H}_2\text{O}]_n \cdot mn \text{H}_2\text{O}\}$, Ln= Nd, m=2 (1), Ln=Ho, m=3 (2), Ln =Er, m=2 (3), Ln=Yb, m=3 (4), $[\text{Tb}_2\text{Co}_2(\mu_3\text{-Hmimda})_2(\mu_3\text{-mimda})_2\cdot 4\text{H}_2\text{O}]_n \cdot 2n\text{H}_2\text{O}$ (5) and $[\text{Dy}_2\text{Co}_2(\mu_3\text{-Hmimda})_2(\mu_3\text{-mimda})_2\cdot 4\text{H}_2\text{O}]_n \cdot n\text{H}_2\text{O}$ (6), (H₃mimda = 1H-2 - methyl-4, 5 -imidazole- dicarboxylic acid) have been developed and characterized. All the complexes (except little disparity of 1) are isostructural and all crystallize in the monoclinic system. They possess an extended reticular-like porous structure constructed from corrugated -shaped 2D layer. Direct current (dc) magnetic susceptibility measurements for 1-5 indicated depopulation of the Stark components at low temperature and /or possible weak anti -ferromagnetic interactions within hetero-nuclear MOFs. The zero field alternating current (ac) susceptibility studies reveal that Dy(III)–Co(II) complex exhibits both possible ferromagnetic couplings and frequency-dependent out-of-phase signals, behaviour of single-ion magnet nature. Fluorescence properties of series complexes both in near-infrared (NIR) and visible region have been comparatively studied.

1. Introduction

In recent years, the rational design and construction of 3d–4f heterometallic coordination polymers have provoked the interest of chemists not only due to their potential applications in the fields of magnetism,¹ luminescence,² gas adsorption,³ and bimetallic catalysis,⁴ but also their fascinating architectures and topologies.^{4,5} From the magnetic viewpoint, molecular magnetic materials based on transition metal ions, such as Co(II) and Mn(II) have been extensively studied because the high spin ground state can be obtained from strong exchange interaction between 3d electrons.^{1b,1d,2d,5b} However, a high spin ground state and significant magneto anisotropy cannot be simultaneously achieved easily in 3d complexes due to a small spin-flip contribution to D (zero-field splitting parameter) in the case of large S (spin quantum number).⁶ On the other hand, lanthanide ions, especially heavier lanthanides such as Tb(III) and Dy(III) are characterized by a large unquenched orbital angular momentum associated with the internal nature of the valence *f* orbitals, giving strong spin–orbital couplings. In principle, they could possess rather large and anisotropic magnetic moments, and thus possibly enhance the coercive fields. The magnetic properties of these lanthanides continue to be an attractive

research field because of their unique and intriguing properties and potential applications in high-density data storage technologies and molecular spintronics. The anisotropic barrier (U) of single- molecule magnet (SMM) is derived from a combination of an appreciable spin ground state and uniaxial Ising-like magneto-anisotropy.⁷ Couplings between the lanthanide and transition metallic ions (*f*–*d*) are much stronger than *f*–*f* interactions, and the combination of such two kinds of spin carriers into a singular material may achieve unexpected properties in heterometallic polymer materials.⁸ Furthermore, lanthanide clusters have shown intense, long-lived emissions, which cover a spectral range from the ultraviolet to the visible, even the near- infrared (NIR) region, such as luminescence from Nd(III), Er(III) and Yb(III) ions are of particular interest because of their potential application in various optical and medical devices.^{1b,2b,2c} As for lanthanide-based fluorescence, the vast majority of this research is focused on the enhancement or quenching of intensity of Ln(III) ions emission and the absorption coefficients are normally very low. One common approach is to conjugate the lanthanide ions to an organic chromophore forming lanthanide chelates, in order to ensure an energy transfer to the lanthanide ion.⁹ Usually, the presence of an aromatic organic system can afford the fully allowed π – π^* transitions, thus result in a possible energy transfer. Recently, hetero-nuclear luminescent

lanthanides have been extensively employed as phosphors, as a new class of luminescent probes for biological applications.¹⁰ This is because that introducing 3d-4f heterometallic units makes the energy levels more controllable, resulting in high efficiencies and photo-luminescence.¹¹ However, to the best of our knowledge, systematic investigation of zeolite-type functional materials containing lanthanide metal atoms series along with the transition metal atoms has been seldom documented hereunto due to the practically challenging syntheses of 3d - 4f heterometallic MOFs.^{1b} Although the coordination polymers based on rigid amide-like ligands containing O and N donor function are widely employed for the assembly of polynuclear 3d species, and are widely characterized structurally,¹² the construction of metal-organic polymers suffers from difficulties in control of heterometallic polymer dimensionality. Especially, little attention has been focused to the coordination chemistry of simple rigid ligand such as imidazole/ pyridine /pyrazine-dicarboxylic acid in luminescent materials. In fact, such ligands are suitable for coordinating 3d-4f metal ions because the chemical characteristics of polydentate can fulfill the coordinating affinities of 3d and 4f metal ions.¹³ In this contribution, we have exploited this approach by preparing multinuclear complexes containing *d*-block luminophore with a vacant N-donor coordination site and carboxylic oxygen as the second coordination site to obtain magnetic and luminescent centers.¹⁴ As continuation of our previous research,¹⁵ we have extended this idea by application of a simple H₃mimda ligand for construction of heterometallic MOFs¹⁶ based on the following considerations: (i) this conjugation system has a rigid sketch and can transit electron facilely; (ii) the functional imidazole group can not merely exhibit collaborative coordination ability with metal ions, but also favour forming supramolecular systems to enhance the thermal stability; (iii) it may be completely or partially deprotonated and has been proven to be able to control the distance between metal ions, resulting in diverse range of coordination geometries.

2. Experimental Section

2.1 Materials and physical measurements

Lanthanide nitrate was prepared by the reaction of lanthanide oxide (purchased from J & K Chemical Limited) with nitric acid (10 mol / L⁻¹). Elemental analyses (C, H and N) were performed on a Perkin-Elmer 2400 element analyzer. IR spectra were recorded in the range 400–4000 cm⁻¹ using a VECTOR-22 spectrometer using KBr discs. Magnetic data were obtained using a Quantum Design MPMS SQUID 7S magneto-meter at an applied field of 2000 Gs using multi-crystalline samples in the temperature range of 1.8–300 K. The magnetic susceptibilities were corrected using Pascal's constant for all the constituent atoms and sample holders. Thermo-gravimetric and differential thermal analysis experiments were performed using a TGA /NETZSCH STA449C instrument heated from 25–900 °C (heating rate of 10°C/min in nitrogen stream). The powder X-ray diffraction (PXRD) patterns were measured at room temperature using a Bruker D8 advance powder diffractometer at 40 kV, 40 mA for Cu K α radiation ($\lambda = 1.5418 \text{ \AA}$), with a scan speed of 0.2 s/step and a step size of 0.02 (2 θ). The data were analyzed for d-

spacing measurements using the EVA program from the Bruker Powder Analysis software package. Absorption spectra were obtained using a Cary 50 Bio UV-visible spectrophotometer (Varian, Inc., Palo Alto, CA) in quartz cuvettes. Luminescence excitation and emission spectra were measured on Edinburgh instrument FLS980 fluorescence spectrometer.

2.2 Procedure for syntheses of a series of heterometallic complexes

The same procedure was employed in preparation the heterometallic complexes **1-4**, hence, complex **1** will be described in details herein. Zinc nitrate hexahydrate (0.0298 g, 0.1 mmol) and 0.1 mmol of lanthanide(III) nitrate hexahydrate, ((**1**) = Nd(NO₃)₃·6H₂O, 0.045 g; (**2**) = Ho(NO₃)₃·5H₂O, 0.043 g, (**3**) = Er(NO₃)₃·6H₂O, 0.046 g, (**4**) = Yb(NO₃)₃·6H₂O, 0.047 g were mixed in a water solution (10 mL) of 1H-2 - methyl-4, 5 - imidazole- dicarboxylic acid (abbreviated as H₃mimda) (0.3 mmol, 0.079 g). After stirring for 30 min in air, the aqueous mixture was placed into 25 mL Teflon-lined autoclave under autogenous pressure being heated at 155 °C for 72 h, and then the autoclave was cooled over a period of 24 h at a rate of 5 °C/h, and pink crystals of (**1**) were obtained suitable for X-ray diffraction analysis. For (**1**), yield: 0.0286 g (47%) based on lanthanide element. Elemental analysis (%): calcd for C₁₂H₁₃N₄NdO₁₁Zn: C 24.06, H 2.18, N 9.35, found: C 24.09, H 2.16, N 9.58. IR (KBr pellet, cm⁻¹): 3511(br), 3040(s), 2893(m), 2360(m), 1612(vs), 1473(s), 1396(s), 883(s), 787(s). For (**2**), yield: 0.0391 g (51%). Elemental analysis (%): calcd for C₁₂H₁₆N₄O_{12.5}HoZn: C 22.29, H 2.49, N 8.66, found: C 22.47, H 2.18 N 8.71 IR (KBr pellet, cm⁻¹): 3510(br), 3146(vs), 2858(s), 1592(s), 1465(vs), 1396(vs), 1160(s), 834(s), 763(s), 746(m). For (**3**), yield: 0.0361 g (54%). Elemental analysis (%): calcd for C₁₂H₁₆ErN₄O_{12.5}Zn: C 22.21, H 2.48, N 8.63, found: C 22.46, H 2.23, N 8.74. IR: 3041(br), 2879(s), 2413(m), 1636(s), 1379(s), 1193(s), 874(m). For (**4**), yield: 0.0321 g (49%). Elemental analysis (%): calcd for C₁₂H₁₆N₄O_{12.5}YbZn: C 22.01, H 2.46, N 8.56, found: C 21.93, H 2.64, N 8.44. IR: 3251(s), 3032(br), 2918 (s), 1630(s), 1572(s), 1463(m), 1367(vs), 1264(m), 854(s). Process of preparations of **5** and **6** are given in Electronic Supporting Information. IR spectra for series of all complexes are reported in Fig. S1, ESI †.

2.3 Crystallographic data collection and refinement

The suitable single crystals of complexes were mounted on a glass fiber using Fomblin Y per- fluoropolyether vacuum oil. Single crystal diffraction data of complexes were collected on a Bruker SMART APEX II CCD diffractometer with graphite-monochromated Mo K α radiation ($\lambda = 0.71073 \text{ \AA}$) at room temperature. The structures were solved using direct methods and successive Fourier difference synthesis (SHELXS-97), and refined using the full-matrix least-squares method on F^2 with anisotropic thermal parameters for all nonhydrogen atoms (SHELXL-97)¹⁷. An empirical absorption correction was applied using the SADABS program.¹⁸ The hydrogen atoms of organic ligands were placed in calculated positions and refined using a riding on attached atoms with isotropic thermal parameters 1.2 times those of their carrier atoms. For complexes **3**, **4** and **5**, the

solvate molecular are difficult to be defined due to high disorder,
so solvate molecules were established by using the program of

5

Table Crystal data and structure refinement for complexes 1-6

Complexes Nos.	1	2	3	4	5	6
Chemical formula	C ₁₂ H ₁₃ N ₄ NdO ₁₁ Zn	C ₁₂ H ₁₆ HoN ₄ O _{12.5} Zn	C ₁₂ H ₁₆ ErN ₄ O _{12.5} Zn	C ₁₂ H ₁₆ N ₄ O _{12.5} YbZn	C ₁₂ H ₁₆ N ₄ O _{12.5} TbCo	C ₁₂ H ₁₅ CoDyN ₄ O ₁₂
Formula weight	598.87	646.59	648.92	654.70	634.14	628.71
Temperature(K)	296(2)	293(2)	293(2)	293(2)	293(2)	293(2)
Crystal system	Monoclinic	Monoclinic	Monoclinic,	Monoclinic	Monoclinic	Monoclinic
Space group	P2(1)/c	C2/c	C/2c	C2/c	C2/c	C2/c
θ Range for collection	1.74- 24.99 °	2.32 - 27.50 °	2.40 - 27.50°	2.32-27.50	2.30 - 27.50°	2.35 - 27.49°
unit cell	a = 12.983(3)	a =24.191(2)	a = 24.2346(14)	a = 24.1744(13)	a = 24.339(3)	a= 24.3237(17)
Dimensions	b = 11.506(3)	b = 9.177(3)	b = 9.1735(5)	b = 9.1789(5)	b = 9.1443(12)	b=9.1523(6)
(Å)	c = 13.013(3)	c =19.010(6)	c = 19.0739(11)	c = 18.9734(10)	c = 19.064(2)	c =19.0813(13)
(°)	β=115.424(4)	β= 113.910(5)	β= 114.1530(1)	β= 114.05	β=114.655(1)	β=114.6250(10)
V(Å ³), Z	1755.6(2), 4	3858(2), 8	3869, 8	3844.6(4), 8	3856.0(9), 8	3861.5(5), 8
μ (mm ⁻¹)	4.361	5.390	5.622	6.158	4.573	4.774
Data/restr /parame	2926/0/264	4388 / 24 / 280	4361 / 24 / 280	4399 / 24 / 280	4402 / 24 / 280	4401 / 12 / 267
ρ (g ml ⁻³)	2.266	2.226	2.228	2.262	2.185	2.194
F(000)	1164	2504	2512	2528	2464	2432
GOF	1.097	1.039	1.029	1.050	1.023	1.101
R ₁ ,wR ₂ [I>2σ(I)]	0.0526, 0.1412	0.0407, 0.1068	0.0301, 0.0846	0.0248, 0.0719	0.0412, 0.0970	0.0423, 0.1240
R ₁ ,wR ₂ (all data)	0.0578, 0.1446	0.0441, 0.1094	0.0327, 0.0867	0.0272, 0.0733	0.0608, 0.1101	0.0485, 0.1286
Residuals (e Å ⁻³)	3.766, -1.147	3.079, -3.573	2.427, -0.946	2.079, -0.981	0.879,-0.864	2.836,-1.152

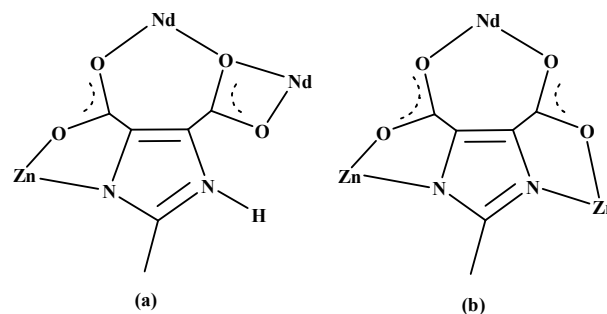
10

$$R = \frac{\sum |F_o| - |F_c|}{\sum |F_o|}, wR = \left\{ \frac{\sum [w(F_o^2 - F_c^2)^2]}{\sum (F_o^2)^2} \right\}^{1/2}$$

PLATON/ SQUEEZE (Spek, 2009) in order to remove the contributions of disordered solvent.¹⁹ Details about the Squeezed material, including the chemical formula, formula weight, final R indices, etc. have been incorporated in cif and/or check report. The summary crystallographic data, structure refinements and selected bond lengths and angles are listed in Table 1, Table S1 and S2, ESI†, respectively. The probable reason for large value of calcd residual density and ADP ratio may indicate unresolved disorder of solvate molecule, which is difficult to identify.

15

20



Scheme 1. Diverse coordination modes of H₂mimda ligand in complex **1**.

3. Results and Discussion

3.1 Description of the structures

The X-ray diffraction analysis reveals that complexes **2–6** are isostructural, and they exhibit very similar basic structure except the distinction of metal ion and different number of water

molecules in crystal lattice. Their stoichiometries have been confirmed by single X-ray crystallography, elements analysis and thermogravimetric analysis. They all crystallize in monoclinic system, with $C2/c$ space group except **1**, which adopts in chiral space group of $P21/c$, containing both Ln(III) and Zn/Co(II) ions. Therefore, only structure of **1** is described here in details as an instance. Fig. 1 (a) gives a perspective view of the basic unit in **1**. The asymmetry unit contains one Nd(III) ion, one zinc (II) ion, four Hmimda ligands and two coordinated waters, as well as two solvate water molecules. The octa-coordinated Nd(III) cation exhibits distorted dodecahedral prism geometry, being accomplished by an O_6N donor set, among which oxygen and nitrogen atoms are all from imidazole-dicarboxylic moieties rather than from water. As far as the Zn(II) ion is concerned, it exhibits a pentahedron geometry, being coordinated by two oxygen atoms from two carboxylic groups and two nitrogen of imidazolyl ring from the next Hmimda ligand, the another oxygen atoms from water occupied the axial position. It just demonstrates slightly different coordination environment from that of simple Zn complex for the bond lengths and angles.²⁰ Two H₃mimda ligands sharing the common Zn(II) ion adopt two categories of

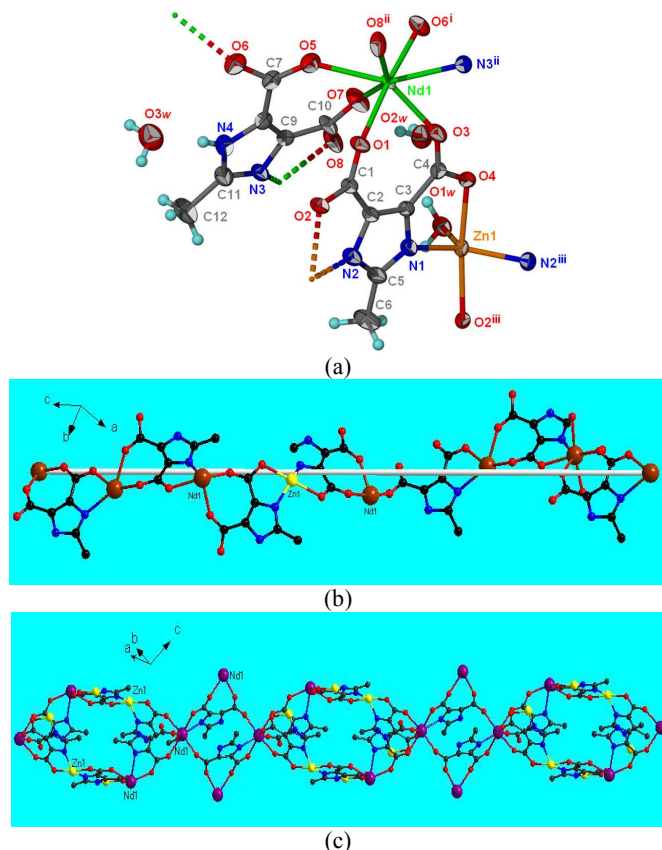


Fig. 1. (a) Coordination environments of the Nd(III) and Zn (II) cations with partial atomic labels in **1**. (Color code: Nd: green; Zn: pink; O: red; N: blue). (b) View of 1-D helical hetero metallic chain structure. (c) View of 1-1D alternate chain composed of tetra-nuclear and hexa-nuclear clusters.

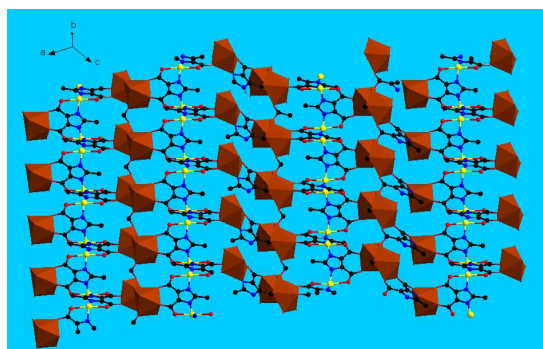
bridging coordination modes. The first one of ligand has been completely protonated for carboxylic group, but an H atom was added to imidazole N, bearing one positive charge. As for the second category, imidazole N has lost a protonate. They are

denoted as $mimda^{2-}$ and $Hmimda^-$, respectively, as illustrated in Scheme 1. The former acts as a pentadentate ligand, and adopts a $\mu_3-kN, O: kO, O': kO, O$ modes connecting two Nd (III) and one Zn (II) centers in bis-(bridging) and cheating mode. The 5-carboxylic group adopts bidentate, monodentate and chelation models. The latter also features a pentadentate ligand, while adopts a $\mu_3-kN, O: kO, O': kN', O'$ mode connecting two Zn(II) and one Nd(III) centers in bis-(bridging) and monodentate modes,

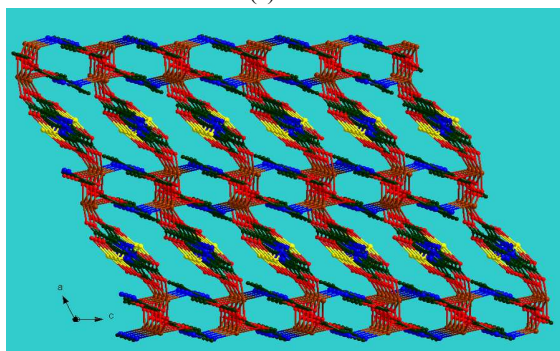
with the shortest separation of Nd-Zn of 6.257 Å. The multidentate functionality of $Hmimda^-$ and the tendency of Ln(III) to have a high coordination number allowed water molecule to act as a terminal ligand to Ln(III) in **1**.²¹ Two adjacent Nd(III) ions are doubly bridged by two 5-carboxylic groups from $Hmimda^-$ ligand to form a dimer unit in an *anti-anti* chelating mode with the separation of Nd...Nd of 6.547 Å. At the same time, the 4, 5-carboxylic groups connect adjacent Zn ions into a binuclear unit with the shortest distance Zn...Zn of 6.09 Å, and it gives rise to 1D helical chain along *ac* plane, as shown in Fig. 1 (b). Four $mimda^{2-}$ ligand alternately linked two adjacent Nd (III) ions and Zn (II) ions into a heterometallic $[NdZn(mimda)_4]$ aggregate as the secondary building unit (SBU) through the carboxylic oxygen and imidazole nitrogen. Meanwhile, two $mimda^{2-}$ ligands connected neighbouring four Nd (III) ions, gives a square lanthanide cluster. The carboxylate further alternately propagates these planar clusters into one dimensional robust polymeric chain approximately along crystallographic *bc* plane, as described in Fig. 1(c).

The carboxylic oxygen atoms crosslink these 1D chains into 2D corrugated-shape layer approximately along crystallographic *ac* plane, as illustrated in Fig. 2(a). Moreover, the carboxylic oxygen and imidazolyl nitrogen atoms from two $mimda$ ligands further interconnected 2D layer sheet, giving rise the finally 3D reticular 3D coordination frameworks, as described in Fig. 2(b). These coplanar rigid ligands always render short separation between adjacent metal ions, facilitating energy transition to the Ln(III) centres, resulting in their potential applications in the areas of magnetic and electroluminescent devices.^{22, 2c, 14} The framework possesses 1D channel along the *c* axis with a window diameter of about 7.55 Å, which is occupied by the both coordinated and solvate water molecules. A series of extensive hydrogen bonding have been found, and details parameters are listed in Table S2, ESI †. This porous assemble is much different from the reported pure lanthanide or pure transition metal complexes based on analogous ligand.²³ As discussed above, H₃mimda ligand acts as three-connected nodes connecting two Nd (III) and one Zn (II) ion, or connecting two Zn (II) ions and one Nd(III) ion. The Nd(III) and Zn(II) are coordinated to three H₃mimda ligands, assuming both Nd(III) ion and H₃mimda ligand act as three-connected nodes, as shown in Fig. 3. Zn (II) is coordinated to two H₃mimda ligands, acting as two-connected nodes. The TOPOS analysis of this network results in a zeolite-like topology with the point number of $\{4^4. 6^2. 4. 4. 4. 4\}$.^{22(c), 23(a)} Total Schläfli symbol is $\{4^2.11^2.12\}$ $\{4.5^2.8^4.10^2.11^3.12^5.14^4\}$, which is also different from other reported hetero-metallic coordination polymers.²⁴ After hypothetical removal of the guest and coordinated waters, the total potential solvent accessible void is found for the 3D

noninterpenetrating framework to be 300.2 \AA^3 per cell volumes (accounting for 17.1 % of the total unit cell system, as volume for $1755.6(8) \text{ \AA}^3$), calculated using the PLATON programmes.²⁵



(a)



(b)

Fig. 2. (a) Polyhedral view of corrugated-shaped 2D layer constructed from Nd_2Zn_2 SBUs. (b) Crystal packing diagram of 3D reticular hetero-metallic framework of **1** along the *a* axis showing existence of 1D channels along the crystallographic *b* axis in porous complex **1**, guest water molecules are not presented for clarity.

It should be pointed that complexes **2-4** crystallize in monoclinic system, and they show slightly different coordination modes from complex **1**, interestingly they are comparable to structures of Co(II) containing complexes **5** and **6**. In **6**, Dy(III) ion adopts just seven coordinated mode with an O_6N_1 donor set, and without water molecules participation in coordination of Co(II). The 5-carboxylic group doubly connects the adjacent two Dy(III) ions. The shortest intermolecular Dy-Dy separation distance is 4.168 \AA , as shown in Fig. S5, ESI, †. Close inspection reveals that there are several obvious strong hydrogen bonding interactions between the oxygen atoms of carboxylic

Compound	Shortest Separation of Ln...Ln (Å)	Shortest Separation of Ln...Zn/Co (Å)	Shortest Separation of Zn...Zn/Co...Co (Å)
----------	------------------------------------	---------------------------------------	--

groups and free water molecules and nitrogen atoms of imidazole rings, and these intra molecular interaction contribute to 3D crystal packing stability. They exhibited different interaction fashions in these family complexes. Similarities of building block in these family hetero-nuclear complexes allow us to compare the metal-ligand distances in the same array, as reported in Table S1, ESI †. Interestingly, comparing the average Ln-N and Ln-O bond lengths among the polymers finds that average lengths of **1-4** display zag-zig like trend with increasing of elements order, as ionic radius of the lanthanide ion become smaller and smaller in the order of Nd(III) > Ho(III) > Er(III) > Yb(III), rather than lanthanide contraction effect.¹⁶ However, separation of Ln...Ln bridged by 4-carboxylate bridging (along *a* axis) and separation of Ln...Zn connected by 5-carboxylic group from mimda ligand do not display the same trend. The reason of inconsistency may be change of Co/Zn coordination mode and the lanthanide contraction effect on the whole series, or the anionic Hmimda ligand having a higher affinity of bonding to the cationic lanthanide ions than the neutral water molecule,²⁶ as listed in Table 2 in details.

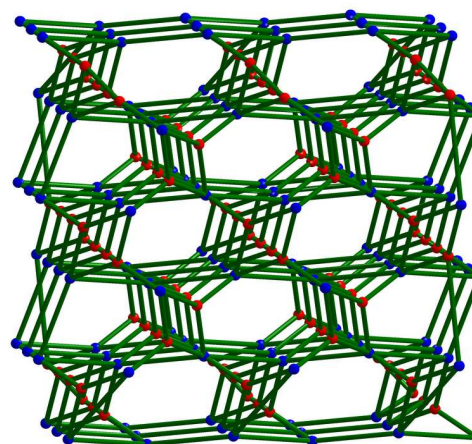


Fig. 3. Topology showing the connectivity between Nd_2Zn_2 nodes. Non-bridging atoms of ligands and hydrogen atoms have been omitted for clarity. Color codes, Zn: blue; Nd: red; Hmimda: green block.

3.2 PXRD patterns and thermal gravimetric analyses

Table 2. Comparing of inter-atomic separations (Å) for series complexes

1 (Nd)	6.547	6.257	6.094
2 (Ho)	4.141	6.228	6.304
3 (Er)	4.144	6.215	6.330
4(Yb)	4.123	6.188	6.326
5(Tb)	4.173	6.311	6.212
6(Dy)	4.167	6.211	6.310

10

The X-ray diffraction powder pattern of the series of complexes **1–6** have been given in Fig. S7 and S8, ESI †, respectively. The powder XRD pattern of the series crystal complexes feature the first hump at $2\theta = 5.68^\circ$ and distinct peaks at $2\theta = 11.2, 14.7, 17.2, 22.4, 24.7$ and 37.4° . The experimental PXRD patterns of bulk samples nearly match with the calculated patterns obtained from

the corresponding single crystal structures. The phase purities of family complexes were confirmed by these comparisons. The PXRD patterns of family complexes are almost identical, indicating that they are isostructural. To characterize the thermal stability of these family complexes, thermo- gravimetric analysis (TG) and differential thermal analysis (DTA) have been carried out, as reported in Fig. S9 and Fig. S10, ESI †. Complexes **1–6** showed the almost similar TG thermal behaviour, and **1** is used to describe as a representative, herein. As indicated in Fig. S9, it shows an endothermic peak in the range of $110\text{--}130^\circ\text{C}$ with a weight loss of 4.44%. This was caused by the release of two lattice water molecules per formula, and the result is close to the theoretical value 4.50 % for per $[\text{Nd}_2\text{Zn}_2(\text{Hmimda})_2(\text{mimda})_2 \cdot 4\text{H}_2\text{O}] \cdot 2\text{H}_2\text{O}$. The second weight loss of ca. 5.48% in the range of $220\text{--}240^\circ\text{C}$ is attentively assigned to release of coordination waters. After the loss of water molecules, the 3D framework was stable up to 430°C and then begins to decompose upon further heating. It also exhibits two exothermic peaks, with a total weight loss of 27.1%, this weight loss is close to the theoretical value (26.3%) calculated for $[\text{Nd}_2\text{Zn}_2(\text{Hmimda})_2(\text{mimda})_2 \cdot 4\text{H}_2\text{O}] \cdot 2\text{H}_2\text{O}$. The larger exothermic peak located at about 440°C with weight loss of 13.9% was probably caused by the decomposition of $[\text{Nd}(\text{Hmimda})]$ moiety. The smaller exothermic peak located at 550°C with weight loss of 23.2% was attentively due to decomposition of $[\text{Zn}(\text{Hmimda})]$ into the ZnO, followed by releasing of CO_2 and H_2O . The complex collapses beyond temperature of 600°C . The residue substance is 39.48% (the calculated ZnO and Nd_2O_3 weight is 39.17%).

3.3 Photoluminescence Properties

Considering the excellent luminescent properties of lanthanide materials,²⁷ the solid state photo luminescent spectra of **1–6** in multi-crystal samples, as well as the free Hmimda ligand were measured at room temperature. The solid-state fluorescence spectra of complexes **1**, **3** and **5** were recorded at room temperature, and reported in Fig.4, Fig.5, Fig. S11- S13, ESI †. The excitation spectra of series complexes were obtained solid by monitoring characteristic transition of Nd(III), Yb(III) and Dy(III) complexes respectively.^{28,29} As displayed in Fig. 4, H₃mimda ligand shows an emission band at 361 nm upon the excitation at 278 nm, which may be assigned to the $\pi^* \rightarrow n$ or $\pi \rightarrow \pi^*$ electron

transition (ILCT).³⁰ The emission spectrum of Er(III) complex **3** bears large similarity with the ones for free ligand, albeit with larger intensity of blue emission maximum at 438 nm, it is also ascribed to ligand centered (ILCT) fluorescence, based on the emission spectrum of free H₃mimda ligand. The maximum peak of complex **3** is slightly redshifted with respect to that of free H₃mimda ligand, which is mainly due to an intraligand $\pi \rightarrow \pi^*$ transition,³¹ being compared with simple zinc complex.³² Interestingly, for **3**, the emission is not the characteristic emission of Er(III) ion, but it is originated from the H₃mimda ligand.³³

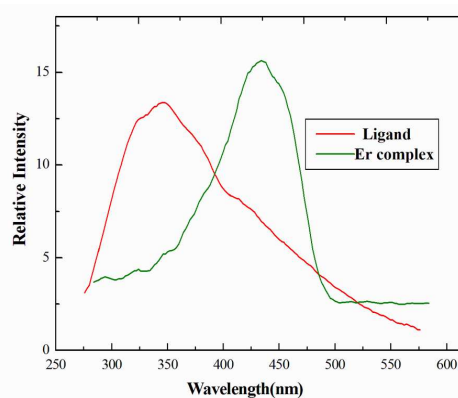
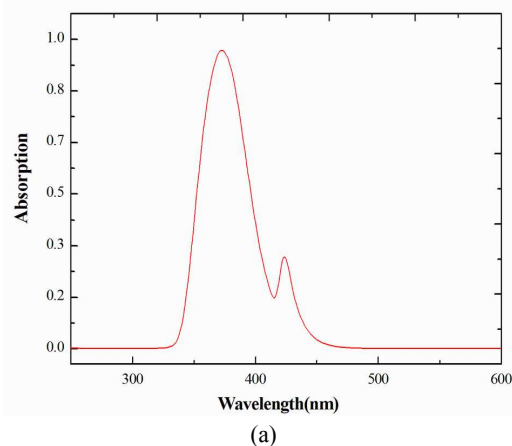


Fig. 4. The room-temperature photoemission spectra of complex **3** (excited at 241 nm) and free H₃mimda ligand in solid state.



75

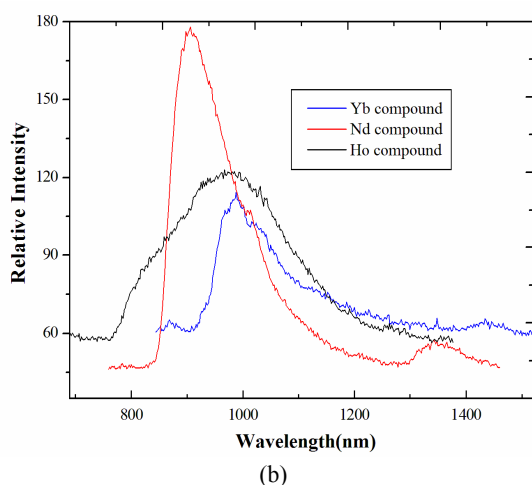


Fig. 5. (a) Absorption spectra (left) for solutions of $[\text{Nd}_2(\text{Zn}_2(\text{Hmimda})_2)]$ (in methanol at pH = 7.2); (b) Emission spectra of **1**, **2**, **4** in the solid state at room temperature.

Upon the excitation maximum at 389 nm, complex **1** displays emission peaks at 911, 1032 and 1342 nm in NIR range, which is attributed to the ${}^4\text{F}_{3/2} \rightarrow {}^4\text{I}_{9/2}$, ${}^4\text{F}_{3/2} \rightarrow {}^4\text{I}_{11/2}$ and ${}^4\text{F}_{3/2} \rightarrow {}^4\text{I}_{13/2}$ characteristic transitions of Nd(III) ion,³⁴ respectively. Based on the Dexter sensitization theory, the ligand will sensitize luminescence ion when corresponding absorb peak is in range of 2100–3100 cm^{-1} . Considering the absorption and emission spectra of complex **1**, as shown in Fig. 5 (a), the UV-vis light characteristic of ligand-centered transitions is absorbed by H_3mimda ligands,³⁵ and the energy is transited to excited states ${}^2\text{P}_{1/2}$ of Nd (III) ions, followed by transition to emitting energy level ${}^4\text{F}_{3/2}$ of Nd(III) ions through intersystem jump. When excited electrons return to ground state level, Nd (III) releases of energy by radiation through antenna effect, exhibiting the characteristic NIR luminescence of Nd(III), as illustrated in Fig. S12, ESI †. The measured fluorescence branching ratios of these transitions are in the order ${}^4\text{I}_{11/2} > {}^4\text{I}_{13/2} > {}^4\text{I}_{9/2} > {}^4\text{I}_{15/2}$ as is typical for Nd (III) based complexes.³⁶ Furthermore, we monitored changes of ionic zinc (II) concentration by using luminescent chemosensory. This is investigated upon titration zinc (II) chloride 1.0 mol/L in $\text{NH}_3 \cdot \text{H}_2\text{O} - \text{NH}_4\text{Cl}$ buffer solution. As displayed in Fig. 6, upon addition of Zn (II), the maximum enhancing of fluorescence intensity at ca 899 nm has occurred. This is perhaps due to the chelation to imidazole and steric effect after introducing Zn chromophore unit entering into the 1D tunnel, followed by enhancement of fluorescence intensity. Furthermore, on increasing the equality, the emission bands in **1** show considerable blue shift that is attributed to approach of the emission maximum of Zn-Hmimda complex. This investigation should facilitate new potential of biological functions with fluorescence microscopy imaging technique, or chemosensor applications. Upon excitation at the maximum absorption of the ligand ($\lambda_{\text{exc}} = 366 \text{ nm}$), the emission spectra of the crystalline samples of **2** exhibit the low intense emission at 874 nm for **2** in the NIR region, as shown in Fig. 7, which is slightly red-shifted (5 nm) compared with that of other water-soluble lanthanide complexes, and it is also be found in spectrum of holmium(III) complex containing 3- hydroxypyridin-2-one.³⁷ Thus, the

emission peaks of **2** may be assigned to ${}^5\text{F}_4 \rightarrow {}^5\text{I}_6$ transition of Ho(III) rather than intraligand fluorescent emissions. The relative weak NIR luminescence intensity of **2** is because that ligand energy is not suitable for electronic energy levels of Ho(III) or due to being quenched by non-radioactive exchange of electronic energy of Ln(III) to the high vibration modes of O-H, C-H oscillators,³⁸ and design and synthesis of nanocrystalline silicon or fully fluorinated chromophore materials is a major challenge in future.^{9b} Upon the irradiation at 397 nm (see Fig. S13, ESI †), one medium strong emission peak was observed for Yb(III) complex maximum at 984 nm, which is attributed to (${}^2\text{F}_{5/2} \rightarrow {}^2\text{F}_{7/2}$) transition of Yb(III) ion, as illustrated in Fig. 5 (blue line). In these systems, the energy is afterward transferred to one or several excited states of the Ln(III) ion, and at last, the metal ion emits light, normally in near-infrared range.³⁹ For this heterometallic complex, UV light is absorbed by the H_3mimda ligands directly coordinated to Zn(II). The Yb luminescence is indeed “lighted up” by excitation of the Zn based chromophores.⁴⁰ Finally, the excimer emission band of Zn complex centred at ca 360 nm (27700 cm^{-1}) can overlap with the absorption bands of H_3mimda ligand, Nd(III) and Yb(III) ions, so that some sensitization of the luminescence of these ions by the heteronuclear framework may occur, either directly or through energy migration onto the $[\text{Hmimda-Zn}]$ subunits. The absorption, excitation, emission spectra of **5** and **6** are reported in Fig. S14, ESI † and Fig. 7, and absorption spectra at wavelengths range of 210–300 nm may be assigned to the $n \rightarrow \pi^*$ or $\pi \rightarrow \pi^*$ electron transitions. As illustrated in Fig. 7, being excited at ca 290 nm, **5** and **6** show similarity of strong emission of free Hmimda ligand peaks at about 400 nm, indicating H_3mimda plays an important role in the emission spectrum, and the emission maximum at ca 400 nm should be attributed to ligand to ligand transition ($\pi \rightarrow \pi^*$ transition) of the Hmimda chromophore. In addition for **5**, the sharp bands at 486, 545 nm are the ${}^5\text{D}_4 \rightarrow {}^7\text{F}_n$ transitions for sensitized terbium emission, where, $n=6, 5$, and the small peaks at 587 and 622 nm are corresponding to ${}^5\text{D}_4 \rightarrow {}^7\text{F}_4$, ${}^5\text{D}_4 \rightarrow {}^7\text{F}_3$ transitions, respectively.⁴¹ However, the emission intensity is quite different from other pure Tb(III) complex with main peaks at 545 nm, since the ligand is not optimum to sensitize Tb (III) ions. T_1 energy level of H_3mimda is much lower than that of ${}^5\text{D}_4$ level of Tb(III), and the reverse energy transfer occurred, resulting in a PL decreases.⁴² For **6** the emission spectrum consists of three main bands at 395, 484 and 577 nm. The emissions maximum at 484 nm and 577 nm are corresponding to ${}^4\text{F}_{9/2} \rightarrow {}^6\text{H}_{13/2}$ and ${}^4\text{F}_{9/2} \rightarrow {}^6\text{H}_{15/2}$ of Dy(III) ions, respectively, and the weak band at ca 667 nm is attributed to the ${}^4\text{F}_{9/2} \rightarrow {}^6\text{H}_{11/2}$ transition.⁴³ Interestingly, this is different from simple Zn complex, and it is less intense than that of Dy-Zn complex.³² This may originate from the deactivation of Co(II) as the paramagnetic cation, resulting in fluorescence quenching.⁴² Among emission peaks, the Ln-Co complex exhibits the strongest emission in green region, originated from ${}^4\text{F}_{9/2} \rightarrow {}^6\text{H}_{13/2}$ transition,⁴⁴ being particularly suitable for generating green light emission.^{43(b)} They display moderate life time values (13.7 ± 1 , $12.4 \pm 1 \mu\text{s}$) for **1** and **3**, respectively because of the poor match of the triplet energy level of H_3mimda ligand with that of ground excited state level.⁴⁵ The intrinsic quantum yield of Ln(III) emission (Φ_{Ln}) can be estimated by $\Phi_{\text{Ln}} = \tau_{\text{obs}}/\tau_0$, where τ_{obs} is the observed emission

lifetime and τ_0 is the “natural lifetime”. It gives value of 42.1% and 37.5% for complex **1** and **3**, respectively. Due to the limitation of our instrument, we were unable to determine τ_{obs} for Er(III) and Ho(III), thus could not estimate Φ_{Ln} for them.

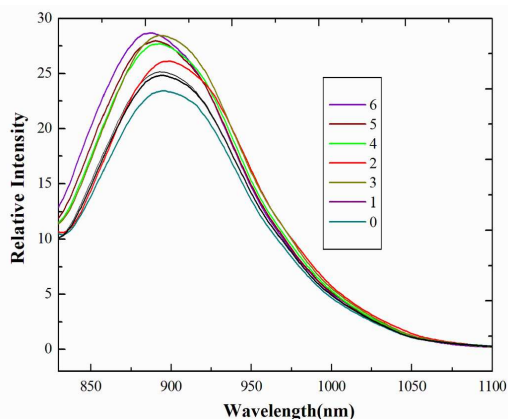


Fig. 6. The plot of the sensing indexes ${}^4F_{3/2} \rightarrow {}^4I_{9/2}$ of Nd(III) ion upon addition of Zn(II) cation (from 0 to 6 equivalents in $\text{NH}_3 \cdot \text{H}_2\text{O}/\text{NH}_4\text{Cl}$ buffer solution at pH = 7.3).

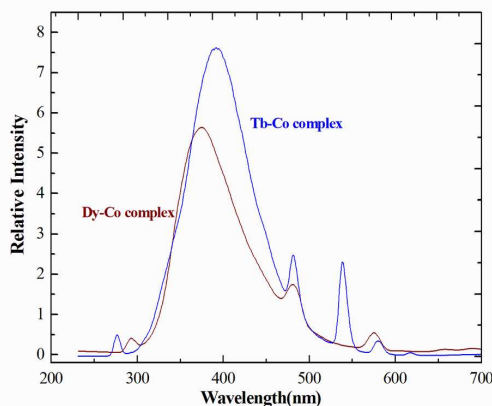


Fig. 7. Excitation spectrum (left) and emission spectrum (right) of **5** and **6** in DMF solvent under room temperature about concentration of 1×10^{-3} mol/L.

3.4 Magnetic properties

The dc magnetic susceptibilities for complexes **1-6** were measured using the polycrystalline samples in an applied direct current (dc) field of 0.20 T. For all complexes, the $\chi_{\text{M}}T$ values display a sharp decrease below 40 K, because the observed decrease of $\chi_{\text{M}}T$ at low temperature may be due to the large anisotropy effects observed for lanthanides. As depicted in Fig. 8 (lower), the $\chi_{\text{M}}T$ value is equal to $1.62 \text{ cm}^3 \text{ K mol}^{-1}$ for **1** at room temperature, which is close to the value expected for an isolated Nd(III) ion ($1.64 \text{ cm}^3 \text{ K mol}^{-1}$), and decreases continuously to a value of $0.56 \text{ cm}^3 \text{ K mol}^{-1}$ at 2 K which is much smaller than the value of $0.61 \text{ cm}^3 \text{ K mol}^{-1}$ expected for an uncoupled Nd(III) ion, indicating an anti-ferromagnetic interaction possibly exists between Nd(III) ions at lower temperature.⁴⁶ This is mainly because of the splitting of the 10-fold degenerate ${}^4I_{9/2}$ ground state by the crystal field and the progressive depopulation of the higher energy, as the temperature is lowered. Notably, the whole profile of the $\chi_{\text{M}}T$ versus T curve is similar to that of reported

mononuclear and homodinuclear complexes,⁴⁷ implying that the magnetic susceptibility of **1** deviates from the Curie law because of the thermal depopulation of Stark level or indicates the presence of possible anti-ferromagnetic interactions between the adjacent Nd(III) cations, or the depopulation of Stark sublevels together with crystal- affection on the consideration of Ln(III) strong spin-orbital coupling.^{29, 47a}

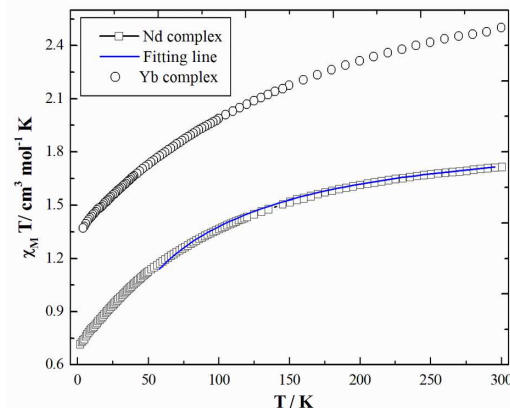


Fig. 8. Temperature dependence of the $\chi_{\text{M}}T$ products at 0.20 T for complexes **1** and **4**. The blue line corresponds to the calculated behaviours of **1** (see the text for details).

Due to the presence of thermally populated excited state, the magnetic property of the neodymium complex **1** remains difficult to interpret even at room temperature, especially for high dimensional system. However, it is possible to extract the value of the spin-orbit coupling constant in the complex by using the analytical approach. Considering magnetic properties is just originated from Ln(III) ions connected by carboxylate bridge, while Zn(II) ion in these complexes does not contribute to magnetic property, and model the magnetic properties of **1** in relative low temperature region involving intramolecular Zn...Nd magnetic interactions can be negligible.⁴⁷ From the magnetic point of view, the basic unit of **1** can also be considered as the mononuclear specie, in which the Nd(III) ions are doubly linked by a pair of carboxylic groups, and the coupling through Hmimda are almost negligible due to the long distance. To obtain a rough quantitative estimation of the magnetic interaction between Ln(III) ions, the Nd(III) ion may be assumed to exhibit a splitting of the m_j energy levels ($\hat{H} = \Delta \hat{J}_z^2$) in an axial crystal field.^{47a, 48} Thus, beyond 30 K the susceptibility data were fitted according to approximately the equation described as eqn (1).

$$\chi_{\text{Nd}} = \frac{N_{\text{g}}^2 \beta^2}{4kT} \times \frac{81e^{-81\Delta/4kT} + 49e^{-49\Delta/4kT} + 25e^{-25\Delta/4kT} + 9e^{-9\Delta/4kT} + e^{-\Delta/4kT}}{e^{-81\Delta/4kT} + e^{-49\Delta/4kT} + e^{-25\Delta/4kT} + e^{-9\Delta/4kT} + e^{-\Delta/4kT}} \quad (1)$$

In these expressions, Δ is the zero-field splitting parameter, and the Zeeman splitting was treated isotropically for the sake of simplicity. The zJ' parameter based on the molecular field approximation in eqn (2) is introduced to take into account the molecular field approximation introduced to simulate the magnetic interaction between the Nd(III) ions.^{47, 26}

$$\chi = \chi_{Nd} / [1 - (2zJ' / Ng^2\beta^2)\chi_{Nd}] \dots\dots\dots (2)$$

The least-squares analysis of the magnetic data gives $\Delta = -1.68 \text{ cm}^{-1}$, $g = 0.78$, $zJ' = -0.49 \text{ cm}^{-1}$ and $R = 2.71 \times 10^{-4}$. For complex **4**, the observed value of $\chi_M T$ per Yb unit is $2.42 \text{ cm}^3 \text{ K mol}^{-1}$ at room temperature (see Fig. 8 upper), which is somewhat smaller than the calculated value ($2.57 \text{ cm}^3 \text{ K mol}^{-1}$) for a free Yb(III) ion. The $\chi_M T$ product decreases slowly as the temperature decreases, to reach a value of $1.36 \text{ cm}^3 \text{ K mol}^{-1}$ at 1.9 K. The decrease of $\chi_M T$ and the negative value of θ are due primarily to the splitting of the ligand field of the Yb(III) ion together with the possible weak antiferromagnetic couplings within the Yb(III)-Zn MOF, considering a possible interaction path through carboxylate bridges with a 4.123 \AA for Yb-Yb distance. The temperature dependence of the reciprocal susceptibilities ($1/\chi_M$) above 25 K obeys the Curie-Weiss law [$\chi_M = C/(T-\theta)$] above 30 K with $\theta = -5.67 \text{ K}$, $C = 2.512 \text{ cm}^3 \text{ K mol}^{-1}$, and $R = 7.71 \times 10^{-4}$, see Fig. S15, ESI †. The negative θ value further supports the presence of weak antiferromagnetic interaction beyond 40 K in **4**.

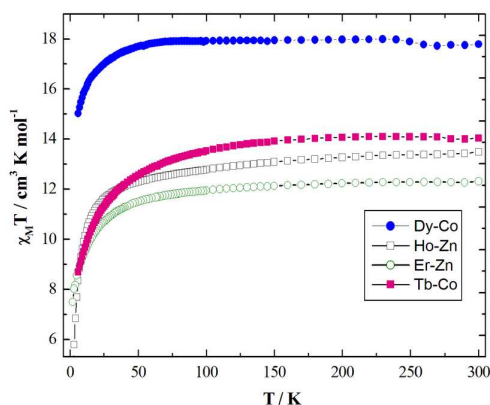


Fig. 9. Plots of the temperature dependence of magnetic susceptibility $\chi_M T$ products for **2**, **3**, **5** and **6**.

The plot of variable-temperature magnetic susceptibility $\chi_M T$ versus T for of **2**, **3**, **5** and **6** are reported in Fig. 9. At 300 K $\chi_M T$ product is equal to $13.42 \text{ cm}^3 \text{ K mol}^{-1}$ for **2**, which is close to the expected value for one isolated Ho(III) ion (with $S = 4/2$, 5I_8 , $g = 4/3$).⁴⁹ For **2**, the χ_M product remains roughly constant between 200–300 K and then drops slightly on lowering temperature down to 50 K, then more dropping sharply down to a low value of $5.7 \text{ cm}^3 \text{ mol}^{-1} \text{ K}$ at 2 K, and similar trends were found for **3** and **5**. As for **2**, **5** and **6**, magnetization measurements in the 0–4.5 T at 2 K are shown in Fig. S16 - S18, ESI †, respectively. Quickly increase of the magnetization even at higher field suggests the possible presence of a magnetic anisotropy and/ or more likely the presence of low-lying excited states expected with the weak Ln...Ln magnetic interactions as discussed above.⁵⁰

At room temperature $\chi_M T$ value is equal to $11.64 \text{ cm}^3 \text{ mol}^{-1} \text{ K}$ for **3**, which is slightly larger than the theoretical value for an independent Er(III) ion spins, $11.48 \text{ cm}^3 \text{ K mol}^{-1}$, (with $S = 15/2$, $g = 6/5$).⁴¹ For complex **5**, $\chi_M T$ value is equal to $13.66 \text{ cm}^3 \text{ mol}^{-1} \text{ K}$, which close to the theoretical values of a free Tb(III) (7F_6 , $S = 3$, $L = 3$, $g = 3/2$, $C = 11.8 \text{ cm}^3 \text{ K mol}^{-1}$) and one Co(II) ion, ($S = 3/2$ ground state, assuming $g = 2.0$). The $\chi_M T$ product value remains

roughly constant beyond 100 K for **2**. Below 100 K, the $\chi_M T$ values decrease dramatically to $8.32 \text{ cm}^3 \text{ K mol}^{-1}$ at 2 K. This behaviour can be attributed to several causes such as: *i*) the thermal depopulation of the Stark sub-levels, *ii*) the presence of significant anisotropy, and *iii*) an antiferromagnetic interaction between the lanthanide ions.^{50, 51} The similar magnetization saturation values were observed for complex **3**. For **2**, fitting of the reciprocal susceptibilities data ($1/\chi_M$) versus temperature according to the Curie-Weiss law results in the $\theta = -0.49 \text{ K}$, $C = 11.46 \text{ cm}^3 \text{ K mol}^{-1}$ and $R = 7.13 \times 10^{-6}$ in whole temperature range, as shown in Fig. S18, ESI †. For **3**, the results are $\theta = -1.43 \text{ K}$, $C = 10.82 \text{ cm}^3 \text{ K mol}^{-1}$ and $R = 8.63 \times 10^{-5}$ in the whole temperature range (Fig. S15, ESI †). For **5**, fitting the data gives negative θ value ($\theta = -2.17 \text{ K}$, $C = 9.82 \text{ cm}^3 \text{ K mol}^{-1}$ and $R = 5.36 \times 10^{-5}$) due to depopulation of Stark levels. It is a challenge to conclude the interactions of Co-Tb and/or Tb-Tb.^{51, 48b}

For **6**, the $\chi_M T$ product at 300 K is $17.08 \text{ cm}^3 \text{ mol}^{-1} \text{ K}$, which is close to the calculated μ_{eff} value expected for an isolated Dy(III) ion ($14.17 \text{ cm}^3 \text{ K mol}^{-1}$): $S=5/2$, $L=5$, $^6H_{15/2}$, $g=4/3$, added to $\chi_M T$ value of $1.87 \text{ cm}^3 \text{ mol}^{-1} \text{ K}$ for a Co(II) ion. As displayed in Fig. 9 (upper), with the temperature is lowered, the $\chi_M T$ value increases steadily and reaches a maximum value of $17.18 \text{ cm}^3 \text{ mol}^{-1} \text{ K}$ at 240 K, and then $\chi_M T$ product remains consistent till 60 K. Then it drops abruptly to a minimum value of $14.94 \text{ cm}^3 \text{ mol}^{-1} \text{ K}$ at 2 K. This is mainly due to the depopulation of the Stark sublevels of the dysprosium ion, which arise from the splitting of the $^6H_{15/2}$ ground term by the ligand field. This is also likely due to crystal-field effects leading to significant magnetic anisotropy. Such behaviour is typical of single ion Dy(III) properties and not necessarily indicative of any antiferromagnetic property. While, beyond 240 K $\chi_M T$ value increase very slowly as the temperature is lowered indicates that existence of weak ferromagnetic coupling between adjacent Dy(III) ions compared with the analogous complexes,³² but is strong enough to overcome the effect of depopulation of the Stark components due to the splitting of free ion ground state by the crystal field.⁴³ Under the inter-electronic repulsion and strong spin-orbit coupling for Dy(III) ions, the $4f^7$ configuration may be split into the $^{2S+1}L_J$ states for **6**. Influenced by the ligand field perturbation, each of these levels may be further split into Stark sublevels, which are thermally populated at room temperature. With decreasing temperature, depopulation of these sublevels will directly cause $\chi_M T$ to drop.⁵² Therefore, the ferromagnetic interaction should exist in **6**, and compensate the decrease of $\chi_M T$ value originated from the depopulation of Stark sublevels on cooling at a higher temperature. Magnetization measurements in the 0–5 T at 2 K were reported in Fig. S18, ESI †, which value increases rapidly with the increasing magnetic field low field and became non-saturation saturated at 0.50 T with value of $8.71 \mu_B$, thus indicating the presence of strong axial anisotropy, but does not reach the expected saturation value of $13 N\beta$ ($10 N\beta$ for each Dy(III) ion for $J = 15/2$, $g = 4/3$, and $3 N\beta$ for one Co(III) ion for $S = 3/2$, $g = 2$).⁵³ For heterometallic complexes **2**, **5** and **6**, the high field linear variation and non-saturation of the magnetization indicates the presence of a significant magnetic anisotropy and/or low lying excited states.⁵⁴ This conclusion is further confirmed by a M vs. $H T^{-1}$ plot (see Fig. S18, ESI †), where the curves are not superimposed on a single master-curve as

expected for an isotropic system with a well defined ground state.⁵⁵

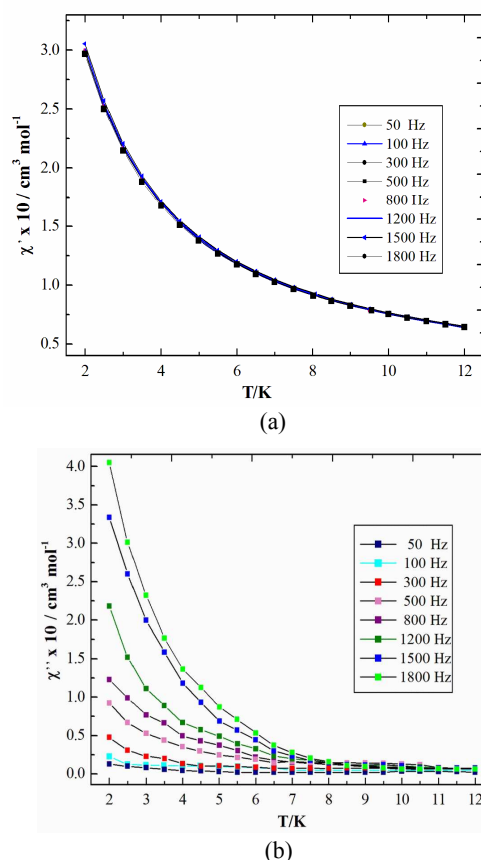


Fig. 10. Temperature dependent in-phase (χ_M') (a) and out-of-phase (χ_M'') (b) AC susceptibility components at different frequencies for Dy-Co complex with zero applied DC field. The solid lines join the data points.

The alternative current (ac) susceptibility was performed on a microcrystalline sample of **6** to investigate the dynamic behaviour of the magnetization at low temperatures. It shows that curves based on in-phase signal of alternating current (ac) susceptibility are superimposed on a single –master curve, as displayed in Fig. 10a. While, obvious frequency-dependent behaviour at the zero fields ranging from 2 to 6 K is observed. The strength of this out-

of-phase signal (χ_M'') in alternating current (ac) susceptibility increases clearly by an order of magnitude and becomes frequency- dependent when a weak external ac field (3 Oe) is applied, showing the strong frequency dependence, suggesting the slow relaxation of the magnetization, as shown in Fig.10(b).

On the other hand, the large spin and the strong magnetic anisotropy of Dy(III) ions due to its high magnitude $\pm m_j$ doubly-degenerate ground state, make them very attractive to design various magnetic materials, including Single-Molecule Magnets (SMM) and Single-Ion Magnets (SIM).⁵⁶ The large intrinsic magnetic anisotropy and the large number of unpaired f-electrons of lanthanide metal ions can contribute to the height of the energy barrier for reversal of magnetization. Currently, the origin of different magnetic behaviors in the dysprosium (III) complexes is still not clear.⁵⁷ However, peaks of ac susceptibility is not

observable even at 1.9 K under the external zero magnetic field, so the blocking temperature is lower than the temperature limit of the magneto meter. To determine the energy barrier and τ_0 , a method employed by Bartolomé,⁵⁸ assuming that there is only one characteristic relaxation process of Debye type with one energy barrier and one time constant, can be used to evaluate the energy barrier and τ_0 roughly based on the following relation (eqn (3)):

$$\ln(\chi_M''/\chi_M') = \ln(\omega\tau_0) + E_a/k_B T \dots \dots \dots (3)$$

As shown in Fig. 10(b), by fitting the experimental χ_M''/χ_M' data to eqn. (3), we extract an estimate of the activation energy of 3.1 K for 1500 Hz, and the characteristic relaxation time of 3.8×10^{-6} s for 1500 Hz.

The series of complexes display different magnetic behaviours, and the divergence mainly originates from the intrinsic natures of different hetero- metallic cluster cores in series complexes. The large and different magnetic anisotropy and complicated Stark energy levels of lanthanide ions in **2**, **5** and **6** from the splitting of individual $^{2S+1}L_J$ states should be responsible for the significant differences of magnetic behaviours for this family complexes.^{48a, 46b, 53a} To best of our knowledge, the coexistence of ferromagnetic coupling and slow magnetic relaxation in hetero-metallic complex **6** is sparsely explored.⁵⁹

4. Conclusions

Series of mixed-metal Zn-4f /Co-4f 3D zeolite-like metal-organic frameworks have been successfully isolated through a new approach and been characterized systematically. Distinct luminescence and magnetic properties are originated from lanthanide ions and short Ln-Zn distances. Complex **1** displays strong characteristic $f-f$ transition luminescence of Nd(III) ion, based on antenna effect arising from H₃mimd ligand, and it may be employed as fluorescence ratiometric probe for Zn(II) ion. Complexes **2**, **4** and **6** exhibit the characteristic luminescence emission in visible or near-infrared regions. The magnetic investigations indicate that the depopulation of Stark levels or possible antiferromagnetic couplings in **1**, **2**, **3** and **4**. Furthermore, the strongest moments are found for the Dy/Co complex, which make them valuable candidates for the design of single- ion magnets. It is believed that the preliminary results presented here may open a promising avenue to rational design of such porous 3d-4f heterometallic coordination polymers based on photochemistry and new materials applicable in single ion magnet.

Acknowledgments

We gratefully acknowledge financial support of this work by the National Natural Science Foundation of China (Nos. 21273101 and 21271098), the Foundation of the Program for Backbone Teachers in Henan Universities, (No. 2012GGJS158), program for Science & Technology Innovation Talents in Universities of Henan Province (2014HASTIT014), the Tackle Key Problem of Science and Technology Project of Henan Province, China (No. 142102310483), and by University of Malaya supporting this study (UM.C/625/1/HIR/247).

Notes and references

- a. College of Chemistry and Chemical Engineering, Luoyang Normal University, Luoyang, 471022, P. R. China. E-mail: fengx@lynu.edu.cn
- b. College of Chemistry and Pharmacy Engineering, Nanyang Normal University, Nanyang, 473601, P. R. China.
- c. Department of chemistry, University of Malaya, Kuala Lumpur, 50603, Malaysia.
- †Electronic Supplementary Information (ESI) available: IR spectra, X-Ray crystallographic files in CIF format CCDC: 973545, 973546, 973547, 973548, 995739 and 973549. The additional structures and characterizations, figures and tables, etc. See <http://dx.doi.org/10.1039/b000000x/>.
- 1 (a) S. J. A. Pope, B. J. Coe, S. Faulkner, E. V. Bichenkova, X. Yu, K. Douglas, *J. Am. Chem. Soc.*, 2004, **126**, 9490; (b) B. Zhao, P. Cheng, X. Y. Chen, C. Cheng, W. Shi, D. Z. Liao, S. P. Yan, Z. H. Jiang, *J. Am. Chem. Soc.*, 2004, **126**, 3012; (c) R. Sessoli and A. K. Powell, *Coord. Chem. Rev.*, 2009, **253**, 2328; (d) M. Andruh, J. P. Costes, C. Diaz and S. Gao, *Inorg. Chem.*, 2009, **48**, 3342.
 - 2 (a) M. D. Ward, *Coord. Chem. Rev.*, 2007, **251**, 1663; (b) B. Zhao, X. Y. Chen, Z. Chen, W. Shi, P. Cheng, S. P. Yan and D. Z. Liao, *Chem. Commun.*, 2009, 3113; (c) L. Aboshyan-Sorgho, C. Besnard, P. Pattison, K. R. Kittilstved, A. Aebischer, J. C. G. Bünzli, A. Hauser and C. Piguet, *Angew. Chem., Int. Ed.*, 2011, **50**, 4108; (d) T. Nishioka, J. L. Yuan, Y. Yamamoto, K. Sumitomo, Z. Wang, K. Hashino, C. Hosoya, K. Ikawa, G. L. Wang, K. Matsumoto, *Inorg. Chem.*, 2006, **45**, 4088; (e) X. F. Li, Y. B. Huang, and R. Cao, *Cryst. Growth Des.*, 2012, **12**, 3549.
 - 3 (a) J. H. Luo, H. W. Xu, Y. Liu, L. L. Daemen, C. Brown, T. V. Timofeeva, S. Q. Ma, H.-C. Zhou, and D.A. Neuman, *J. Am. Chem. Soc.*, 2008, **130**, 9626; (b) P. Mahata, K. V. Ramya and S. Natarajan, *Inorg. Chem.*, 2009, **48**, 4942; (c) Y. Wang, M. Fang, Y. Li, J. Liang, W. Shi, J. Chen, P. Cheng, *Int. J. Hydrogen Energ.*, 2010, **35**, 8166.
 - 4 (a) M. Fang, B. Zhao, Y. Zuo, J. Chen, W. Shi, J. Liang and P. Cheng, *Dalton Trans.*, 2009, 7765-7770, (b) X. L. Hu, C. Y. Sun, C. Qin, X. L. Wang, H. N. Wang, E. L. Zhou, W. E. Li and Z. M. Su, *Chem. Commun.*, 2013, **49**, 3564; (c) A. D. Dias, S. Viswanathan, *Chem. Commun.*, 2004, 1024; (d) C. M. G. dos Santos, P. B. Fernandez, S. E. Plush, J. P. Leonard, T. Gunnlaugsson, *Chem. Commun.*, 2007, 3389.
 - 5 (a) T. Devic, C. Serre, N. Audebrand, J. Marrot and G. Férey, *J. Am. Chem. Soc.*, 2005, **127**, 12788-12790; (b) B. Abrahams, N. Fitzgerald, R. Robson, *Inorg. Chem.*, 2010, **49**, 5953; (c) S. V. Eliseeva and J. C. G. Bünzli, *Chem. Soc. Rev.*, 2010, **39**, 189; (d) X. D. Zhu, Z. J. Lin, T. F. Liu, B. Xu, and R. Cao, *Cryst. Growth Des.*, 2012, **12**, 4708.
 - 6 (a) S. Osa, T. Kido, N. Matsumoto, N. Re, A. Pochaba, J. Mrozinski, *J. Am. Chem. Soc.*, 2004, **126**, 420; (b) M. H. Zeng, M. X. Yao, H. Liang, W. X. Zhang, X. M. Chen, *Angew. Chem. Int. Ed.*, 2007, **46**, 1832; (c) L. F. Zou, L. Zhao, Y. N. Guo, G. M. Yu, Y. Guo, J. K. Tang, Y. H. Li, *Chem. Commun.*, 2011, **47**, 8659; (d) L. Gregoli, C. Danieli, A. L. Barra, P. Neugebauer, G. Pellegrino, G. Poneti, R. Sessoli, A. Cornia, *Chem. Eur. J.*, 2009, **15**, 6456.
 - 7 B. L. Chen, M. Eddaoudi, S. T. Hyde, M. O'Keeffe, O. M. Yaghi, *Science*, 2001, **291**, 1021. Kosuke Suzuki, Rinta Sato and Noritaka Mizuno, *Chem. Sci.*, 2013, **4**, 596.
 - 8 (a) Y. Z. Zhang, G. P. Duan, O. Satob and S. Gao, *J. Mater. Chem.*, 2006, **16**, 2625; (b) T. D. Pasatoiu, J. P. Sutter, A. M. Madalan, F. Z. Fellah, C. Duhayon, and M. Andruh, *Inorg. Chem.*, 2011, **50**, 5890; (c) D. Phanon, Y. Suffren, M. B. Taouti, D. Benbental, A. Breniere and I. Gautier-Luneau, *J. Mater. Chem. C*, 2014, **2**, 2715.
 - 9 (a) S. I. Klink, L. Grave, D. N. Reinhoudt, and F. C. J. M. van Veggel, *J. Phys. Chem. A*, 2000, **104**, 5457; (b) H. Q. Ye, Z. Li, Y. Peng, C. C. Wang, T. Y. Li, Y. X. Zheng, A. Sapekin, G. Adamopoulos, I. Hernández, P. B. Wyatt, W. P. Gillin, *Nature Mater.*, 2014, **13**, 382; (c) X. Feng, X. L. Ling, B. Liu, Z. Q. Shi, J. J. Shang, L. Y. Wang, *Inorg. Chem. Commun.*, 2012, **15**, 1.
 - 10 (a) Q. Sun, Q. Yue, J. Y. Zhang, L. Wang, X. Li, E. Q. Gao, *Cryst. Growth Des.*, 2009, **9**, 2310; (b) Stephen Faulkner, Louise S. Natrajan, William S. Perry and Daniel Sykes, *Dalton Trans.*, 2009, 3890; (c) R. D. Poulsen, M. R. V. Jorgensen, J. Overgaard, F. K. Larsen, W. G. Morgenroth, T. Graber, Y. S. Chen, B. B. Iversen, *Chem. Eur. J.*, 2007, **13**, 9775.
 - 11 (a) Y. Cui, Y. Yue, G. Qian and B. Chen, *Chem. Rev.*, 2011, **112**, 1126; (b) J. P. West, W. L. Queen, S. J. Hwu and K. E. Michaux, *Angew. Chem., Int. Ed.*, 2011, **50**, 3780.
 - 12 (a) X. F. Zhang, T. L. Hu, X. H. Bu, *Dalton Trans.*, 2008, **56**; (b) J. P. Zhao, B. W. Hu, Q. Yang, X. F. Zhang, T. L. Hu, X. H. Bu, *Dalton Trans.*, 2010, **56**; (c) A. X. Zhu, J. B. Lin, J.-P. Zhang, X.-M. Chen, *Inorg. Chem.*, 2009, **48**, 3882; (d) Y. Y. Lin, Y. B. Zhang, J. P. Zhang, X. M. Chen, *Cryst. Growth Des.*, 2008, **10**, 3673; (e) G. P. Yang, Y. Y. Wang, A. Y. Liu, Y. N. Fu, J. C. Zhang, Jin and Q. Z. Shi, *Cryst. Growth Des.*, 2010, **10**, 1443.
 - 13 (a) K. C. Szeto, K. O. Kongshaug, S. Jakobsen, M. Tilset, K. P. Lillerud, *Dalton Trans.*, 2008, **15**, 2054; (b) E. D. Bloch, D. Britt, C. Lee, C. J. Doonan, F. J. Uribe-Romo, H. Furukawa, J. R. Long, O. M. J. Yaghi, *Am. Chem. Soc.*, 2010, **132**, 14382; (c) C. Wang, W. B. J. Lin, *Am. Chem. Soc.*, 2011, **133**, 4232; (d) T. Jacobs, M. J. Hardie, *Chem. Eur. J.*, 2012, **18**, 267; (e) M. Fang, P. F. Shi, B. Zhao, D. X. Jiang, P. Cheng, W. Shi, *Dalton Trans.*, 2012, **41**, 6820.
 - 14 (a) L. Bogani, W. Wernsdorfer, *Nat. Mater.*, 2008, **7**, 179; (b) P. Zhang, L. Zhang, S. Y. Lin, and J. K. Tang, *Inorg. Chem.*, 2013, **52**, 6595.
 - 15 (a) C. V. K. Sharma, G. A. Broker, J. G. Huddleston, J. W. Baldwin, R. M. Metzger, R. D. Rogers, *J. Am. Chem. Soc.*, 1999, **121**, 1137; (b) R. Kitaura, G. Onoyama, H. Sakamoto, R. Matsuda, S. Noro, S. Kitagawa, *Angew. Chem. Int. Ed.*, 2004, **43**, 2684.
 - 16 X. Feng, Y. Q. Feng, L. Liu, L. Y. Wang, H. L. Song and S. W. Ng, *Dalton Trans.*, 2013, **42**, 7741.
 - 17 (a) G. M. Sheldrick, SHELXS 97, *Program for the Solution of Crystal Structure*, University of Göttingen, Germany 1997; (b) G. M. Sheldrick, SHELXL 97, *Program for the Crystal Structure Refinement*, University of Göttingen, Germany 1997.
 - 18 G. M. Sheldrick, *SADABS Siemens Area correction Absorption Program*; University of Göttingen; Göttingen, Germany, 1994.
 - 19 (a) S. Lipstman, S. Muniappan, I. Goldberg, *Cryst. Growth Des.*, 2008, **8**, 1683; (b) X. Feng, J. G. Wang, B. Liu, L. Y. Wang, J. S. Zhao, S. W. Ng, *Cryst. Growth Des.*, 2012, **12**, 927.
 - 20 (a) J. F. Song, R. S. Zhou, T. P. Hu, Z. Chen, B. B. Wang, *J. Coord. Chem.*, 2010, **63**, 4201; (b) K. Z. Shao, Y. H. Zhao, X. L. Wang, Y. Q. Lan, D. J. Wang, Z. M. Su, and R. S. Wang, *Inorg. Chem.*, 2009, **48**, 10.
 - 21 H. L. C. Feltham, Y. Lan, F. Klöwer, L. Ungur, L. F. Chibotaru, A. K. Powell and S. Brooker, *Chem. Eur. J.*, 2011, **17**, 4362. H. L. C. Feltham, Y. Lan, F. Klöwer, L. Ungur, L. F. Chibotaru, A. K. Powell and S. Brooker, *Chem. Eur. J.*, 2011, **17**, 4362.
 - 22 (a) H. B. Xu, Y. T. Zhong, W. X. Zhang, Z. N. Chen, X. M. Chen, *Dalton Trans.*, 2010, **39**, 5676; (b) N. Weibel, L. J. Charbonniere, M. Guardigli, A. Roda, and R. J. Zeissel, *J. Am. Chem. Soc.*, 2004, **126**, 4888; (c) Z. G. Gu, H. C. Fang, P. Y. Yin, L. Tong, Y. Ying, S. J. Hu, W. S. Li and Y. P. Cai, *Cryst. Growth Des.*, 2011, **11**, 2220.
 - 23 X. Feng, L. F. Ma, L. Liu, L. Y. Wang, H. L. Song, and S. Y. Xie, *Cryst. Growth Des.*, 2013, **13**, 4469.
 - 24 (a) S. R. Batten, S. M. Neville, D. R. Turner, *Coordination Polymers: Design, Analysis and Application*; Royal Society of Chemistry: Cambridge, 2009; (b) Y. G. Sun, Y. L. Wu, G. X. Philippe, F. Smet, F. Ding, M. Y. Guo, M. C. Zhu, E. J. Gao, D. Poelman, and F. Verpoort *Dalton Trans.*, 2010, **39**, 11383.
 - 25 The calculation of the solvent-accessible was performed by using the PLATON software (similarly hereinafter); Spek, A. L. *J. Appl. Crystallogr.*, 2003, **36**, 7.
 - 26 Z. H. Zhang, Y. Song, T. Okamura, Y. Hasegawa, W. Y. Sun and N. Ueyama, *Inorg. Chem.*, 2006, **45**, 2896.
 - 27 K. Hanaoka, K. Kikuchi, H. Kojima, Y. Urano, T. Nagano, *J. Am. Chem. Soc.*, 2004, **126**, 12470.
 - 28 (a) G. Mancino, A. J. Ferguson, A. Beeby, N. J. Long, T. S. J. Jones, *Am. Chem. Soc.*, 2005, **127**, 524; (b) N. M. Shavaleev, R. Scopelliti, F. Gumy, J. C. G. Bünzli, *Inorg. Chem.*, 2009, **48**, 2908; (c) K. A. White, D. A. Chengelis, M. Zeller, S. J. Geib, J. Szakos, S. Petoud, N. L. Rosi, *Chem. Commun.*, 2009, 4506.
 - 29 X. Feng, L. Liu, L. Y. Wang, H. L. Song, Z. Q. Shi, X. H. Wu, S. W. Ng, *J. Solid State Chem.*, 2013, **206**, 277.

- 30 (a) V. A. Montes, R. Pohl, J. Shinar and P. J. Anzenbacher, *Chem. Eur. J.*, **2006**, *12*, 4523. (b) L. M. Leung, W. Y. Lo, S. K. So, K. M. Lee and W. K. Choi, *J. Am. Chem. Soc.*, **2000**, *122*, 5640.
- 31 (a) Y. Q. Sun, J. Zhang, Y. M. Chen and G. Y. Yang, *Angew. Chem. Int. Ed.*, **2005**, *44*, 5814; (b) P. Shao, X. Y. Kuang and L. P. Ding, *J. Phys. Chem. A.*, **2013**, *117*, 12998.
- 32 X. Feng, S. B. Miao, T. F. Li, and L. Y. Wang, *Russ. J. Coord. Chem.*, **2011**, *37*, 572.
- 33 M. Fujii, M. Yoshida, S. Hayashi, K. Yamamoto, *J. Appl. Phys.*, **1998**, *84*, 4525.
- 34 (a) J. W. K. Lo, W. K. Wong, W. Y. Wong, J. P. Guo, K. T. Yeung, Y. K. Cheng, X. Yang, and R. A. Jones, *Inorg. Chem.*, **2006**, *45*, **23**, 9321; (b) D. Yang, Y. Dai, P. Ma, X. Kang, M. Shang, Z. Cheng, C. Li, and J. Lin, *J. Mater. Chem.*, **2012**, *22*, 20618.
- 35 (a) K. A. White, D. A. Chengelis-Czegany, M. Zeller, S. J. Geib, J. Szakos, S. Petoud and N. L. Rosi, *Chem. Commun.*, **2009**, 4506; (b) P. Wang, J. P. Ma, Y. B. Dong, R. Q. Huang, *J. Am. Chem. Soc.*, **2007**, *129*, 10620.
- 36 B. F. Moore, T. J. Emge, and J. G. Brennan, *J. Am. Chem. Soc.*, **2005**, *127*, 15900.
- 37 (a) S. Quici, M. Cavazzini, G. Marzanni, G. Accorsi, N. Armaroli, B. Ventura, F. Barigelletti, *Inorg. Chem.*, **2005**, *44*, 529; (b) E. G. Moore, G. Szigethy, J. Xu, L. O. Plsson, A. Beeby and K. N. Raymond, *Angew. Chem. Int. Ed.*, **2008**, *47*, 9500.
- 38 (a) J. C. G. Bünzli and C. Piglet, *Chem. Soc. Rev.*, **2005**, *34*, 1048; (b) J. Feng and H. J. Zhang, *Chem. Soc. Rev.*, **2013**, *42*, 387.
- 39 (a) E. Junior, N. B. D. J. *Mol. Model.*, **2005**, *12*, 16; (b) de Sa', G. F. Malta, O. L. Donega, C. D. Simas, A. M. Longo, R. L. Santa-Cruz, P. A. da Silva, E. F. *Coord. Chem. Rev.*, **2000**, *196*, 165; (c) A. de Bettencourt-Dias, S. Viswanathan, *Dalton Trans.*, **2006**, 4093.
- 40 (a) L. S. Natrajan, W. S. Perry and D. Sykes, *Dalton Trans.*, **3890**; (b) L. S. Natrajan, P. L. Timmins, M. Lunn and S. L. Heath, *Inorg. Chem.*, **2007**, *46*, 10877; (c) W. K. Wong, H. Z. Liang, W. Y. Wong, *New J. Chem.*, **2002**, *26*, 275.
- 41 T. L. Esplin, M. L. Cable, H. B. Gray, and A. Ponce, *Inorg. Chem.*, **2010**, *49*, 4643.
- 42 H. Xin, M. Shi, X. C. Gao, Y. Y. Huang, Z. L. Gong, D. B. Nie, H. Cao, Z. Q. Bian, F. Y. Li, and C. H. Huang, *J. Phys. Chem. B.*, **2004**, *108*, 10796.
- 43 J. Pisarska, L. Zur, W. A. Pisarski, *Spectrochim Acta A Mol Biomol Spectrosc.*, **2011**, *79*, 705.
- 44 (a) A. S. Holmes, K. Suhling, D. J. Birch, *Biophys Chem.*, **1993**, *48*, 193; (b) X. D. Guo, G. S. Zhu, Z. Y. Li, F. X. Sun, Z. H. Yang and S. L. Qiu, *Chem. Commun.*, **2006**, 3172.
- 45 (a) N. M. Shavaleev, S. J. A. Pope, Z. R. Bell, S. Faulkner, M. D. Ward, *Dalton Trans.*, **2003**, 808 ; (b) G. A. Hebbink, D. N. Reinhoud, F. C. van Veggel, J. M. *Eur. J. Org. Chem.*, **2001**, 4101.
- 46 (a) M. Andruh, E. Bakalbassis, O. Kahn, J. C. Trombe, P. Porcher, *Inorg. Chem.*, **1993**, *32*, 2, 1616; (b) H. W. Hou, G. Li, L. K. Li, Y. Zhu, X. R. Meng, Y. T. Fan, *Inorg. Chem.*, **2003**, *42*, 428; (c) L. Cañadillas-Delgado, J. Pasández- Molina, O. Fabelo, M. Hernández-Molina, F. Lloret, M. Julve, C. Ruiz-Pérez, *Inorg. Chem.*, **2006**, *45*, 10585.
- 47 (a) N. Xu, W. Shi, D. Z. Liao, S. P. Yan, P. Cheng, *Inorg. Chem.*, **2008**, *47*, 8748; (b) O. Kahn, *Molecular Magnetism*, VCH Publishers, New York, 1993.
- 48 (a) R. Feng, L. Chen, Q. H. Chen, X. C. Shan, Y. L. Gai, F. L. Jiang and M. C. Hong, *Cryst. Growth. Des.*, **2011**, *11*, 1705; (b) M. Andruh, I. Ramade, E. Codjovi, O. Guillou, O. Kahn, J. C. Trombe, *J. Am. Chem. Soc.*, **1993**, *115*, 1822; (c) C. Benelli, and D. Gatteschi, *Chem. Rev.*, **2002**, *102*, 2369.
- 49 P. F. Yan, F. M. Zhang, G. M. Li, J. W. Zhang, W. B. Sun, M. Suda, Y. Einaga, *J. Solid State Chem.*, **2009**, *182*, 1685.
- 50 (a) Y. F. Yuan, T. Cardinaels, K. Lunstroot, K. V. Hecke, L. V. Meervelt, C. Goirler-Walrand, K. Binnemans, and P. Nockemann, *Inorg. Chem.*, **2007**, *46*, 5302; (b) D. F. Weng, X. J. Zheng, X. B. Chen, L. C. Li, and L. P. Jin, *Eur. J. Inorg. Chem.*, **2007**, 3410; (c) G. Abbas, Y. H. Lan, G. E. Kostakis, W. Wernsdorfer, C. E. Anson, and A. K. Powell, *Inorg. Chem.*, **2010**, *49*, 8067; (d) L. N. Dawe, K. V. Shuvaev and L. K. Thompson, *Inorg. Chem.*, **2009**, *48*, 3323.
- 51 N. M. Randell, M. U. Anwar, M. W. Drover, L. N. Dawe and Laurence K. Thompson, *Inorg. Chem.*, **2013**, *52*, 6731.
- 52 (a) Y. Wang, X. L. Li, T. W. Wang, Y. Song and X. Z. You, *Inorg. Chem.*, **2010**, *49*, 969; (b) M. Fang, B. Zhao, Y. Zuo, J. Chen, W. Shi, J. Liang and P. Cheng, *Dalton Trans.*, **2009**, 7765.
- 53 (a) N. Ishikawa, M. Sugita, T. Ishikawa, S. Koshihara, Y. J. Kaizu, *Phys. Chem. B.*, **2004**, *108*, 11265; (b) P. H. Lin, T. J. Burchell, R. Clerac, M. Angew. Murugesu, *Chem. Int. Ed.*, **2008**, *47*, 8848.
- 54 (a) J. Tang, I. Hewitt, N. T. Madhu, G. Chastanet, W. Wernsdorfer, C. E. Anson, C. Benelli, R. Sessoli and A. K. Powell, *Angew. Chem. Int. Ed.*, **2006**, *45*, 1729; (b) Y. Z. Zheng, Y. Lan, C. E. Anson and A. K. Powell, *Inorg. Chem.*, **2008**, *47*, 10813; (c) M. T. Gamer, Y. Lan, P. W. Roesky, A. K. Powell and R. Clerac, *Inorg. Chem.*, **2008**, *47*, 6581; (d) J. M. Zhou, W. Shi, N. Xu, and P. Cheng, *Cryst. Growth Des.*, **2013**, *13*, 1218.
- 55 S. K. Langley, N. F. Chilton, B. Moubaraki, and K. Murray, *Inorg. Chem.*, **2013**, *52*, 7183.
- 56 (a) N. Ishikawa, M. Sugita, T. Ishikawa, S. Koshihara and Y. Kaizu, *J. Am. Chem. Soc.*, **2003**, *125*, 8694; (b) J. D. Rinehart, K. R. Meihaus and J. R. Long, *J. Am. Chem. Soc.*, **2010**, *132*, 7572; (c) M. Jeletic, P. H. Lin, J. J. Leroy, I. Korobkov, S. I. Gorelsky and M. Murugesu, *J. Am. Chem. Soc.*, **2011**, *133*, 19286; (d) S. D. Jiang, S. S. Liu, L. N. Zhou, B. W. Wang, Z. M. Wang and S. Gao, *Inorg. Chem.*, **2012**, *51*, 3079.
- 57 (a) Y. Z. Zheng, Y. H. Lan, C. E. Anson and A. K. Powell, *Inorg. Chem.*, **2008**, *47*, 10813; (b) Z. He, E. Q. Gao, Z. M. Wang, C. H. Yan, M. Kurmoo, *Inorg. Chem.*, **2005**, *44*, 862.
- 58 J. Bartolome, G. Filoti, V. Kuncser, G. Schinteie, V. Mereacre, C. E. Anson, A. K. Powell, D. Prodius, *Phys. Rev B.*, **2009**, *80*, 014430.
- 59 Z. Chen, B. Zhao, P. Cheng, X. Q. Zhao, W. Shi and Y. Song, *Inorg. Chem.*, **2009**, *48*, 3493.

Electronic Supporting Information for Dalton. Trans.

Reticular three-dimensional 3d–4f frameworks constructed through substituted imidazole–dicarboxylate: syntheses, luminescence and magnetic properties study

Xun Feng,^{a,*} Yu-Quan Feng^b, Jun Jing Chen^b, Seik-Weng Ng^c, Li-Ya Wang,^{b,*,*} and Jin-Zhong Guo,^a

a. College of Chemistry and Chemical Engineering, Luoyang Normal University, Luoyang, 471022, P. R. China.

b. College of Chemistry and Pharmacy Engineering, Nanyang Normal University, Nanyang, 473601, P. R. China.

c. Department of chemistry, University of Malaya, Kuala Lumpur, 50603, Malaysia

E-mail: fengx@lynu.edu.cn, wlya@lynu.edu.cn

1. Additional experimental section

1.1. Synthesis of complexes 5 and 6

Cobalt nitrate hexahydrate (0.0292 g, 0.1 mmol) and 0.1 mmol of lanthanide (III) nitrate hexahydrate, Tb(NO₃)₃·6H₂O (0.042g), (**5**); Dy(NO₃)₃·6H₂O, 0.046 g (**6**) were mixed in a ethanol-water solution (10 mL) of H₃mimda (0.3 mmol, 0.079 g). After stirring for 30 min in air, the aqueous mixture was placed into 25 mL Teflon-lined autoclave under autogenous pressure being heated at 165 °C for 90 h, and then the autoclave was cooled over a period of 24 h at a rate 5 °C/h. pale red crystals were obtained suitable for X-ray diffraction analysis. For (**5**), yield: yield: 0.0241 g (38%) based on Ln element. Elemental analysis (%): calcd for C₁₂H₁₆CoN₄O_{12.5}Tb: C 22.72, H 2.54, N 8.83, found: C 21.85, H 2.43, N 8.75. IR: 3352(s), 3030 (br), 2859(s), 2150(m), 1716(s), 1613(s), 1572(vs), 1430(s), 1117(m), 1009(s), 789(s). For red crystals of (**6**), yield: 0.0325 g (51%). Elemental analysis (%): calcd for C₁₂H₁₅CoDyN₄O₁₂: C 22.92, H 2.41, N 8.91, found: C 22.85, H 2.43, N 8.79. IR: 3402(s), 3028(br), 2909 (s), 2100(m), 1711(s), 1621(s), 1495(vs), 1380(s), 1078(s), 822(s).

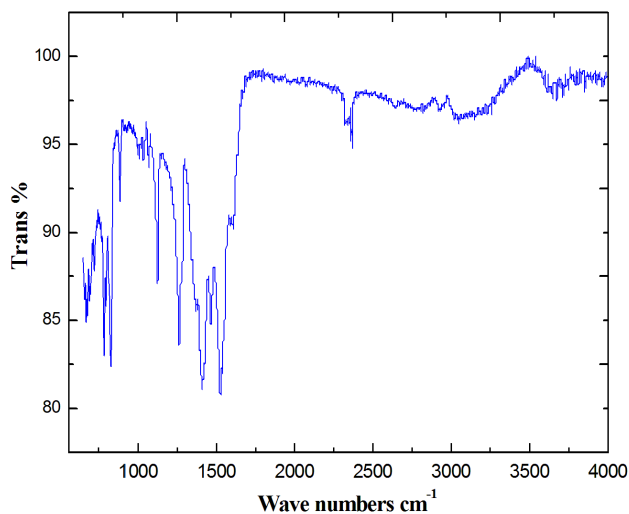
1.2. About fluorescence method

For fluorescence titrations, a stock solution of the sensor was prepared as the same as UV-vis luminescence spectra. The solutions of the guest cations using the 0.5mol/L ZnCl₂ salts in the order of 1 to 6 equates were prepared in deionized water. Solutions of ZnCl₂ salts were prepared separately in

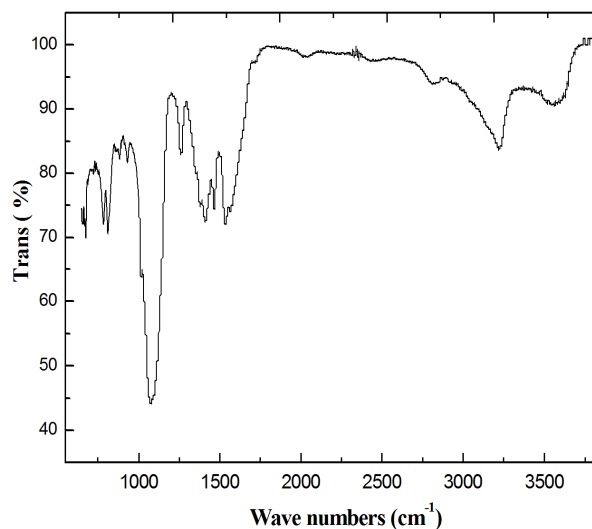
$\text{NH}_3 \cdot \text{H}_2\text{O}/\text{NH}_4\text{Cl}$ buffer solution at $\text{pH} = 7.3$. The spectra of these solutions were recorded by means of fluorescence methods through microliter syringe adding the ZnCl_2 solution at 0.1 ml once time. The luminescence quantum yield measurements were obtained with a Fluorolog-3 Horiba Jobin Yvon equipped with a Hamamatsu R928P photomultiplier with a SPEX 1934 D phosphorimeter and a xenon lamp at room temperature, from 1×10^{-4} mol/L chloroform solutions at an excitation wavelength of *ca* 360 nm, with a slit width of 1.0 nm for the excitation, and 1.0 nm for the maximum emission, with a Horiba Quanta-Q F-3029 integrating sphere mounted in the sample.

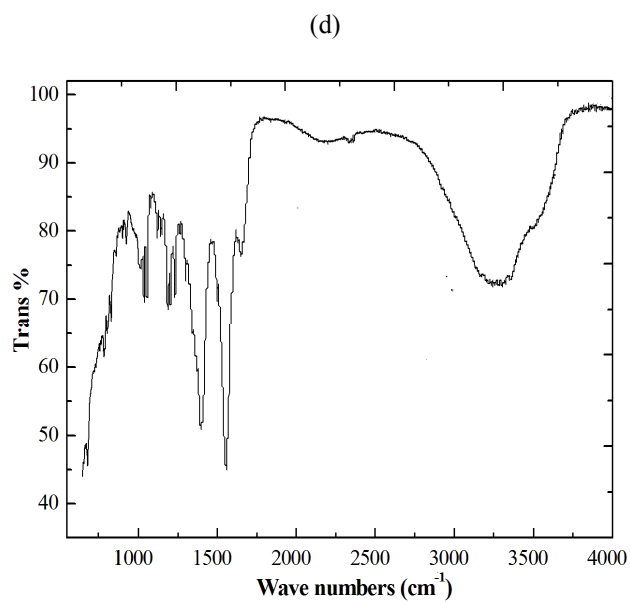
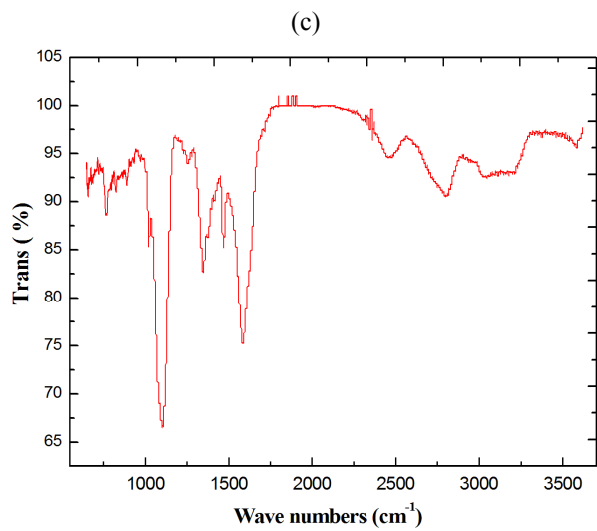
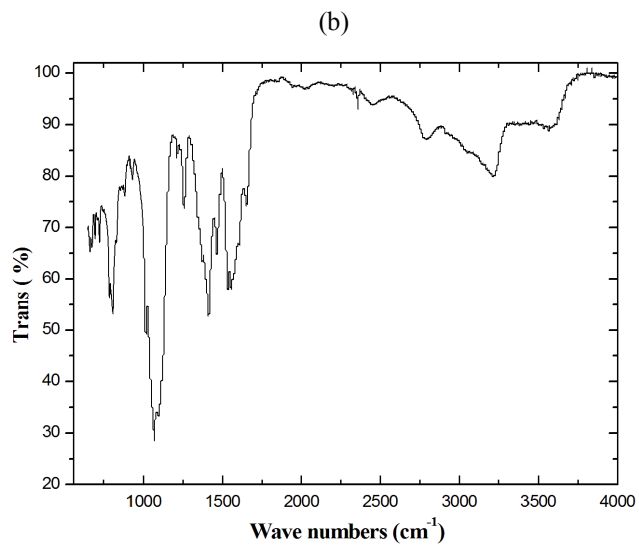
2. Addition discussions and results

2. 1. IR spectra of complexes 1-6



(a)





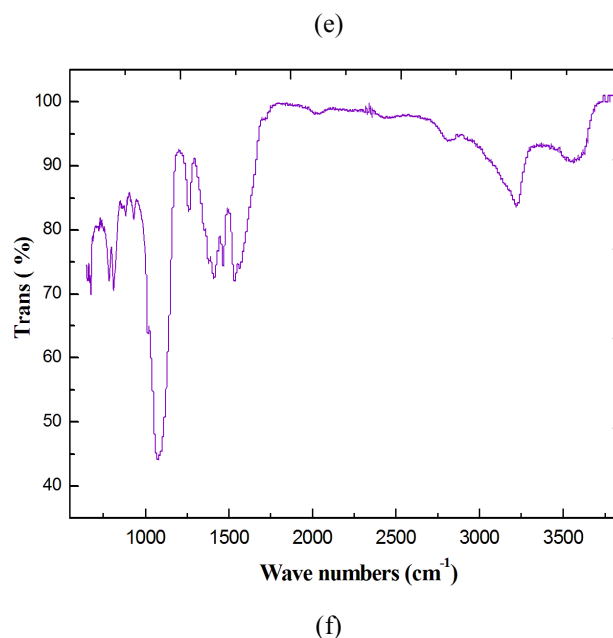


Fig. S 1. IR spectra for compounds **1**(a), **2**(b), **3**(c), **4**(d), **5** (e) and **6** (f)

2. 1. Comparison of the Structures of 1-6

The X-ray diffraction analysis (owing to the less optimum quality of data measurements, a number of restraints were used in the refinements) reveals that compounds **2** -**6** are isostructural, even if compounds **5** and **6** feature different transition metals. They all crystallize in monoclinic system, with $C2/c$ space group. The perspective view of **2** with atom labeling scheme is illustrated in Fig. S2. The asymmetry unit contains one Ho(III) ion, one zinc (II) ion, four Hmimda ligands, and two coordinated water molecules as well as two solvate water molecules. The octa-coordinated Ho(III) cation exhibits distorted dodecahedral prism geometry, being accomplished by an O_8 donor set, among which two oxygen atoms are from water molecules, and six are from imidazole carboxylate. As far as the Zn(II) ion is concerned, it exhibits a octahedron geometry, being coordinated by four oxygen atoms from two carboxylic groups and two nitrogen of imidazole ring from the next mimda ligand. It just demonstrates slightly different coordination environment being compared with the pure Zn(II) compound for the bond lengths and angles.^{1,2} Two dicarboxylate ligands sharing the common Zn (II) ion adopt two types of bridging coordination modes, but all in chelating bridging bidentate fashions. The first category has been completely deprotonated for carboxyl group, but an H atom was added to imidazole N bearing one positive charge, and the

imidazole N in the second category has been deprotonated. They are denoted as mimda^{2-} and Hmimda^- , respectively. The 5-carboxylic group adopts bidentate, monodentate and chelated modes. The Hmimda^- ligand, while adopts a μ_3 - $kN, O: kO, O': kN', O'$ modes connecting two Zn(III) and one Ho(III) centers in bis-(bridging) and monodentate modes. In this structure, the shortest separation of Ho-Zn is 6.274 Å, as illustrated in Fig .S2.

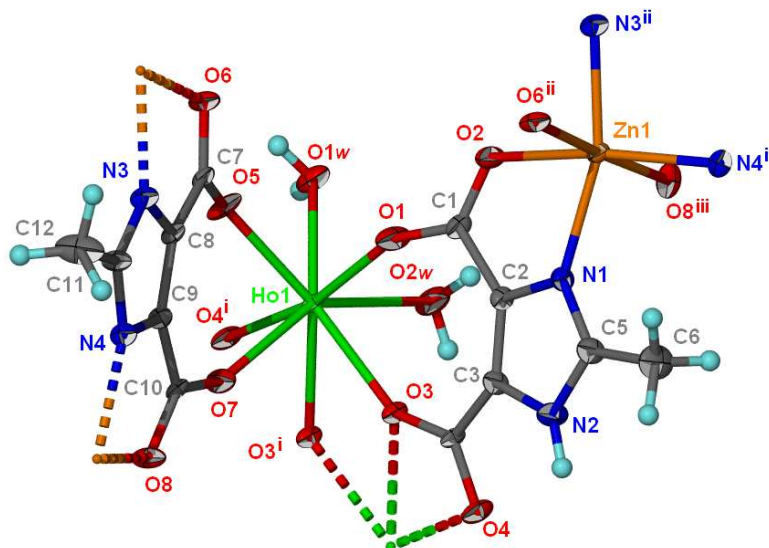


Fig. S2. (a) Coordination environments of the Ho(III) and Zn (II) cation with partial atomic labels in **2**

Two Ho(III) ions and four Zn(II) ions are combined by two μ_3 - Hmimda ligands to produce a heterometallic hexanuclear $[\text{Ho}_2\text{Zn}_4(\text{Hmimda})_4]$ as second building unit, rather than tetranuclear ring-like aggregate, as displayed in Fig S4. These hexanuclear clusters are grafted on to an infinite 1D double-stranded structure H_3mimda ligand acts as three- connected nodes connecting two Ho (III) and one Zn (II) ion, or connecting two Zn (II) ions and one Ho (III) ion. Both Ho (III) and Zn (II) are coordinated to three H_3mimda ligands, assuming both the metal cation and H_3mimda ligand act as three- connected nodes, as shown in Figure. S6. The TOPOS analysis of this network results in a zeolite-like topology with the point number of $(4.8^2)(8^2.12)$. Total Schläfli symbol is $\{3;4;5^2;6;7; 8^2; 11^2;12^4;13\} \{4^3;8; 10^2; 12^3;14^3;15;16;17\}$, which is similar to reported analogous hetero-metallic coordination polymers.⁴

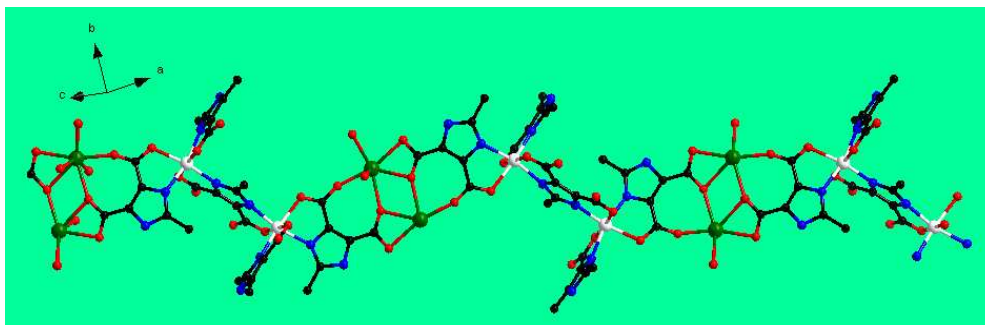


Fig. S3. 1D zig-zag chain assembled from alternate sub-units based upon Ho(III) (green) and Zn(II) (white) ions.

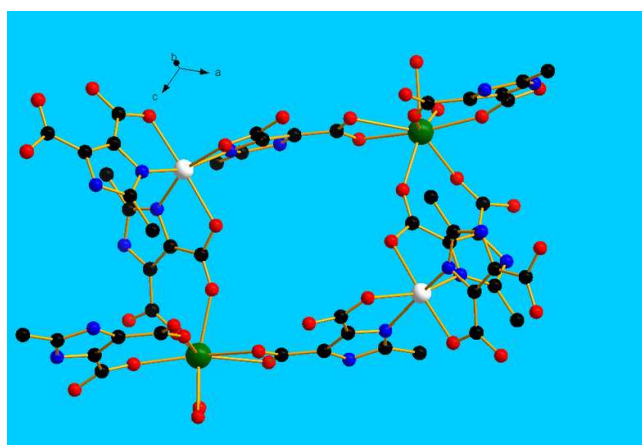


Fig. S4. Illustration of an individual Ho₂Zn₂ parallelogram fragment linked by Hmimda ligands viewed approximately down the *bc* plane in **2**. Color codes: Ho(III), green; Zn, white.

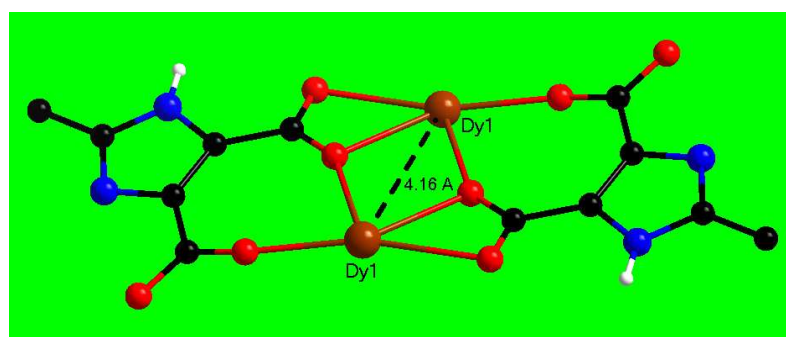


Fig. S5. Illustration of two adjacent Dy(III) ions doubly connected by 4-carboxylic group from Hmimda ligands viewed approximately down *ac* plane in **6**.

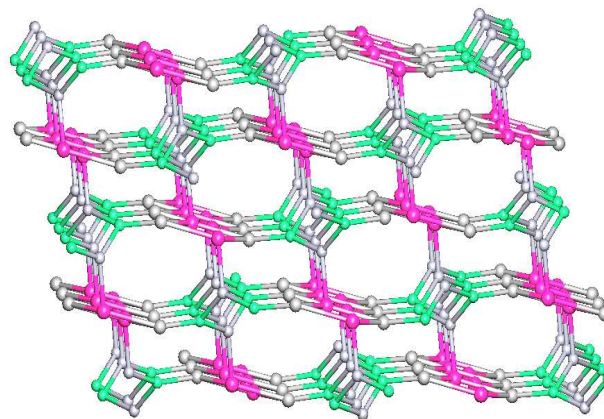


Fig. S6. Topology showing the connectivity between three linking nodes in **2**. Non-bridging atoms of ligands and hydrogen atoms have been omitted for clarity. Color codes, Co: green; Ho: purple; Hmimda ligand: gray.

1.3 Additional PXRD and thermal deposition property

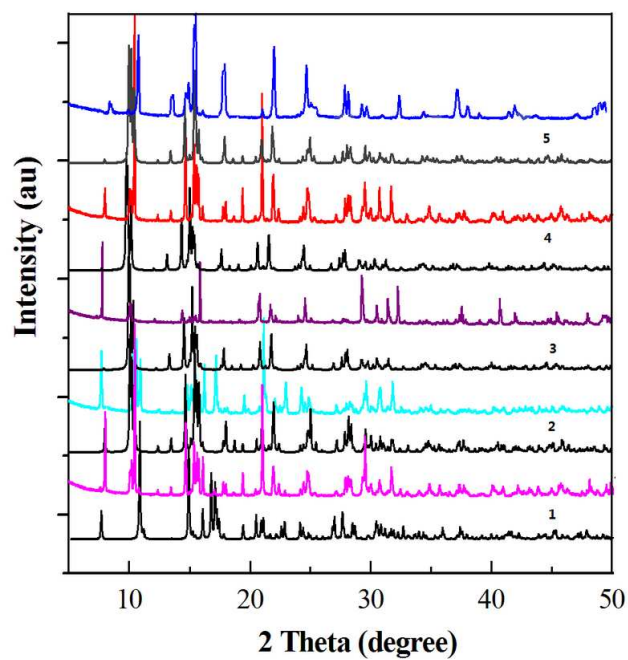


Fig. S7. Comparing the simulated XRD (all in black) and experimental PXRD patterns of compounds **1-5** (presented by pink, cyan, purple, red and blue pattern, respectively)

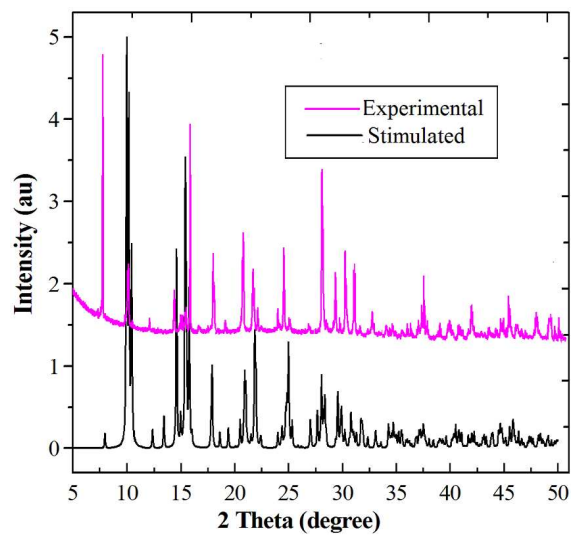


Fig. S8. Comparing the simulated PXRD and experimental PXRD of 6

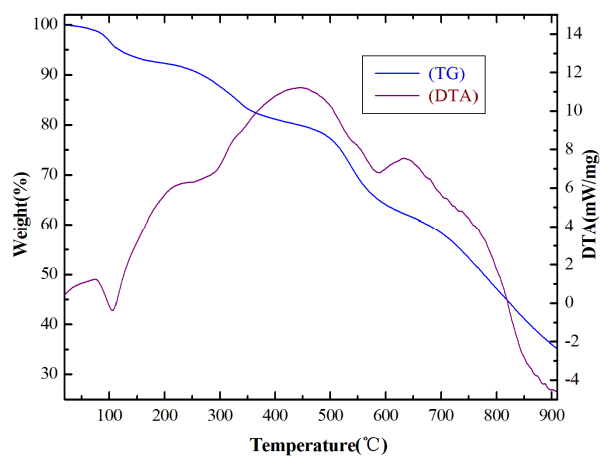


Fig. S9. The TGA curves for complex 1

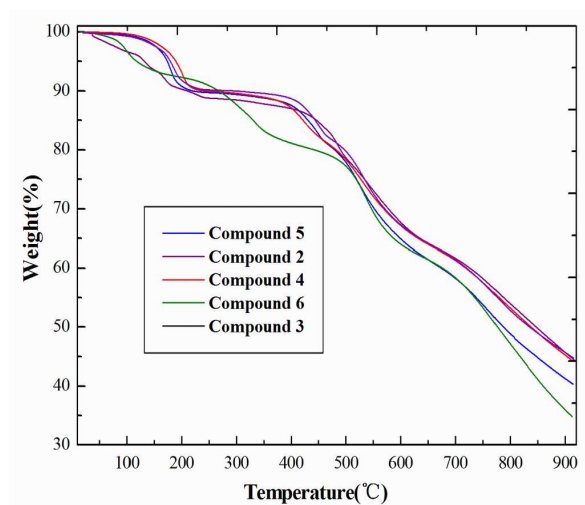


Fig. S10. The TG analysis curves for complexes 2- 6.

Photoluminescence Property of Zn complex

The photoluminescence properties of $[\text{Zn}(\text{Hmimda})_2]$ in the methanol suspension samples (ca. 0.001 mol/L) were investigated at room temperature. As shown in Fig. S11, upon photo-excitation at 326 nm the emission spectra showed the intense emission bands ranging from 400 to 430 nm in purple regions with a maximum wavelength of 414 nm. In comparison with the emission of the free H₃mimda ligand ($\lambda_{\text{max}} = 372$ nm) in a methanol solution at room temperature, the fluorescence of zinc compound has a red shift, which may be assigned to the metal ligand charge transfer (MLCT)⁴. The coordination of the ligand to the metal ion increases the rigidity of molecular edifice and shows intense fluorescence due to the presence of relatively rigid conjugated systems such as imidazole ring.

3. Additional Figures

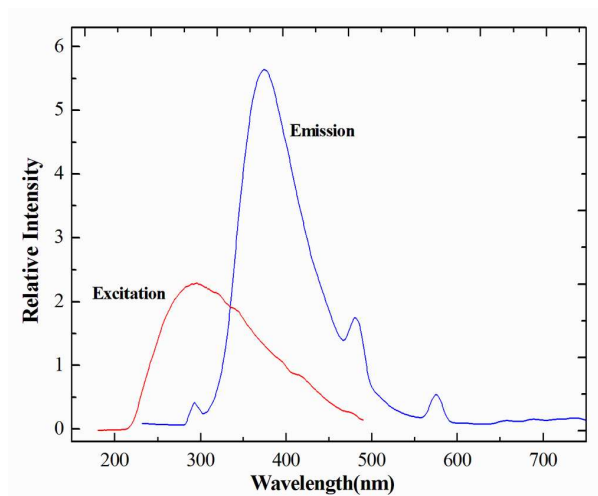


Fig. S11. PL excitation and emission spectra of Zn-Hmimda complex in the methanol suspension.

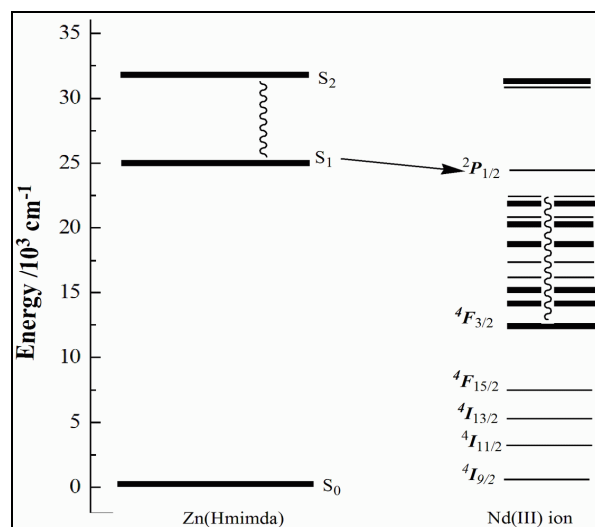


Fig. S12. Schematic representation of the energy flow paths during sensitization of Nd(III) ion luminescence via the [Zn-Hmimda] unit.

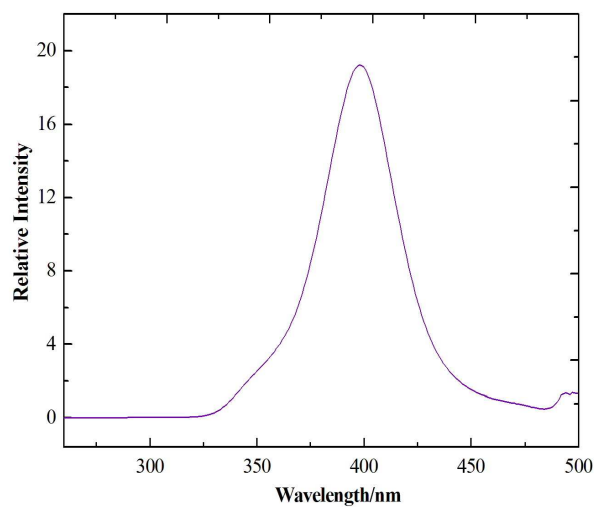


Fig. S13. The excitation spectrum of **4** normalized on emission at 900 nm.

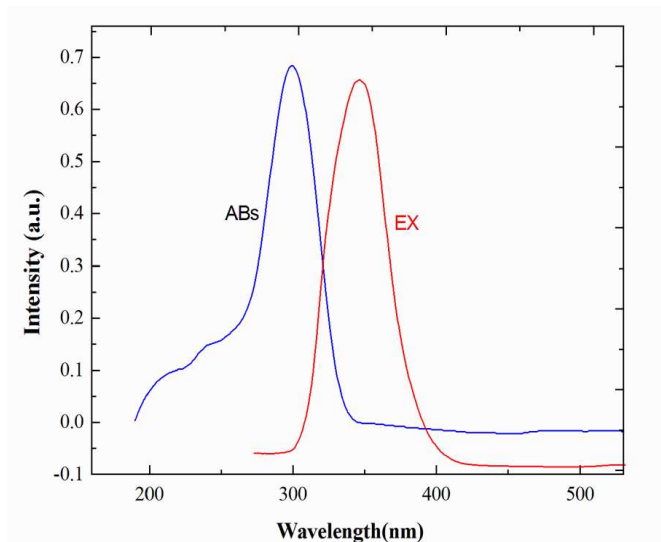
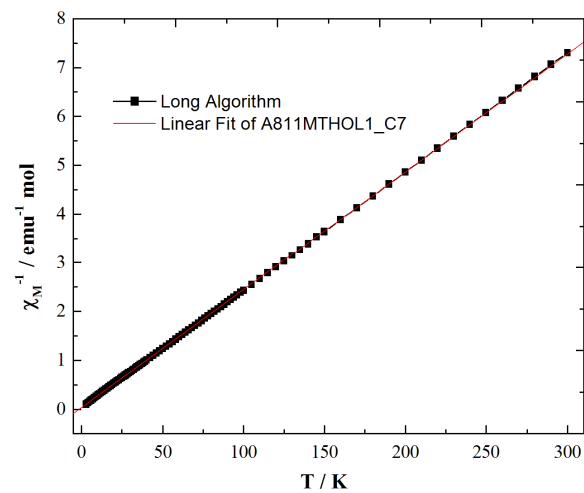
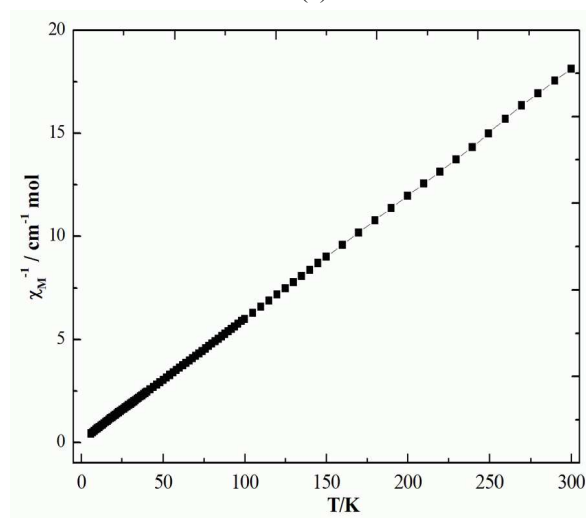


Fig. S14. Photophysical analysis of polymer **6** in methanolic suspension: absorbance spectrum (blue) and excitation spectrum (red) normalized on emission at 576 nm.



(a)



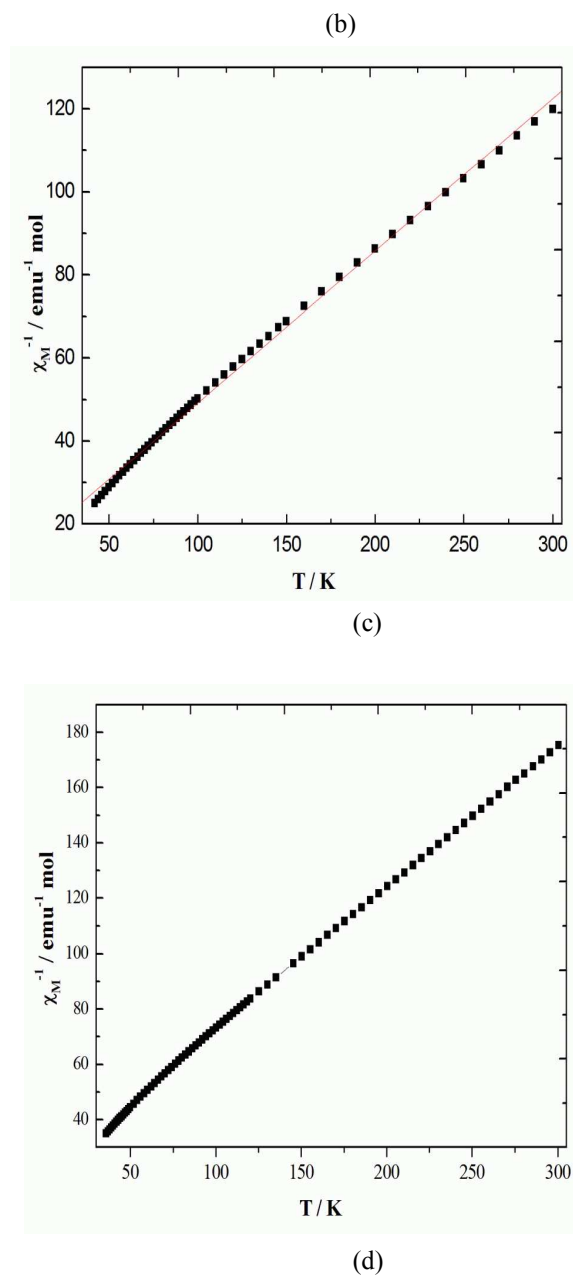


Fig. S 15. Plot of inverse molar susceptibility against temperature under a 0.2 T field for **2** (a), **3** (b), **4** (c), **5** (d), the Solid lines present the best fit indicated in the text.

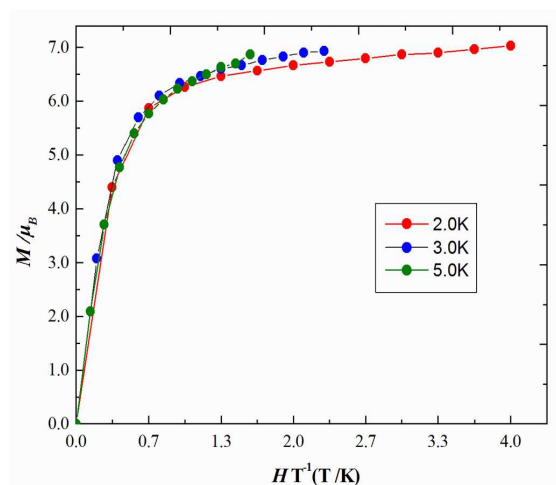


Fig. S 16. Magnetization plots (M vs H/T) from 2 to 5 K for **2** after the sample being heated

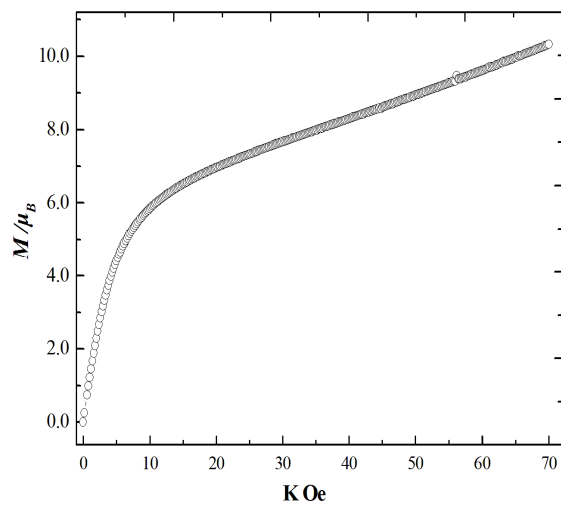


Fig. S 17. Magnetization plots (M vs H/T) for **5** at 2 K.

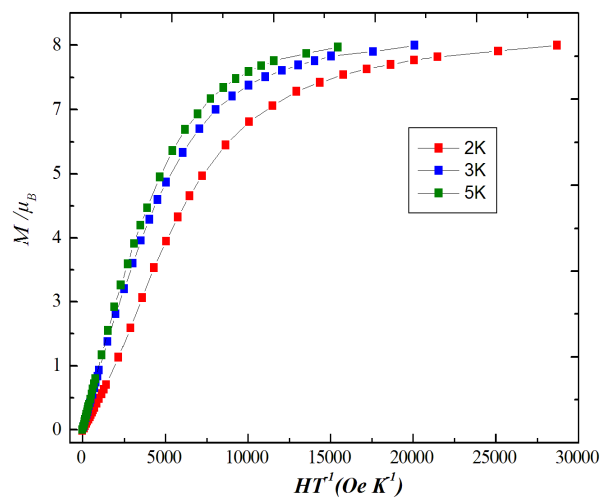


Fig. S 18. Magnetization plots (M vs H/T) for **6** from 2 to 5 K

1.2. Additional Tables:

Table S1 Selected bond lengths [\AA] and angles [$^\circ$] for complexes **1–6**

Complex 1					
Bond	Length	Bond	Length	Bond	Length
Bond	Length	Bond	Length	Bond	Length
Nd(1)-O(1)	2.241(7)	Nd(1)-O(7)	2.300(7)	Zn(1)-O(4)	2.156(6)
Nd(1)-O(3)	2.213(7)	Nd(1)-O(8)#2	2.322(7)	Zn(1)-O(1w)	1.992(8)
Nd(1)-O(5)	2.342(8)	Nd(1)-N(3)#2	2.568(8)	Zn(1)-N(1)	1.992(8)
Nd(1)-O(6)#1	2.264(8)	Zn(1)-O(2)#3	2.213(6)	Zn(1)-N(2)#3	1.988(8)
Bond	Angle	Bond	Angle	Bond	Angle
O(3)-Nd(1)-O(1)	80.9(3)	O(1)-Nd(1)-O(5)	78.9(3)	N(2)#3-Zn(1)-O(1w)	110.7(4)
O(3)-Nd(1)-O(6)#1	91.8(3)	O(6)#1-Nd(1)-O(5)	104.9(3)	N(1)-Zn(1)-O(1w)	110.9(3)
O(1)-Nd(1)-O(6)#1	171.2(3)	O(7)-Nd(1)-O(5)	74.5(3)	N(2)#3-Zn(1)-O(4)	95.8(3)
O(3)-Nd(1)-O(7)	77.1(3)	O(8)#2-Nd(1)-O(5)	73.4(2)	N(1)-Zn(1)-O(4)	79.5(3)
O(1)-Nd(1)-O(7)	94.0(3)	O(3)-Nd(1)-N(3)#2	75.6(3)	O(1w)-Zn(1)-O(4)	94.1(3)
O(6)#1-Nd(1)-O(7)	79.6(3)	O(1)-Nd(1)-N(3)#2	105.0(3)	N(2)#3-Zn(1)-O(2)#3	78.2(3)
O(3)-Nd(1)-O(8)#2	135.1(3)	O(6)#1-Nd(1)-N(3)	77.5(3)	N(1)-Zn(1)-O(2)#3	101.8(3)
O(1)-Nd(1)-O(8)#2	86.6(3)	O(7)-Nd(1)-N(3)#2	143.5(3)	O(1w)-Zn(1)-O(2)#3	92.4(3)
O(6)#1-Nd(1)-O(8)#2	102.1(3)	O(8)#2-Nd(1)-N(3)	66.4(2)	O(4)-Zn(1)-O(2)#3	172.4(3)
O(7)-Nd(1)-O(8)#2	147.1(3)	O(5)-Nd(1)-N(3)#2	139.1(2)	O(3)-Nd(1)-O(5)	143.5(2)
Complex 2					
Bond	Length	Bond	Length	Bond	Length
Ho(1)-O(1)	2.218(4)	Ho(1)-O(3)#1	2.517(3)	O(3)-Ho(1)#1	2.517(3)
Ho(1)-O(5)	2.278(4)	Zn(1)-N(3)#2	2.052(5)	O(4)-Ho(1)#1	2.434(4)
Ho(1)-O(7)	2.281(4)	Zn(1)-N(4)#3	2.067(5)	O(6)-Zn(1)#2	2.210(4)
Ho(1)-O(2w)	2.316(4)	Zn(1)-N(1)	2.113(5)	O(8)-Zn(1)#4	2.247(4)
Ho(1)-O(1w)	2.393(4)	Zn(1)-O(2)	2.168(4)	N(3)-Zn(1)#2	2.052(5)
Ho(1)-O(3)	2.400(4)	Zn(1)-O(6)#2	2.210(4)	N(4)-Zn(1)#4	2.067(5)
Ho(1)-O(4)#1	2.434(4)	Zn(1)-O(8)#3	2.247(4)	O(3)-Ho(1)#1	2.517(3)
Bond	Angle	Bond	Angle	Bond	Angle
O(1)-Ho(1)-O(5)	78.43(17)	O(1w)-Ho(1)-O(3)	146.32(13)	N(3)#2-Zn(1)-N(1)	162.39(18)
O(1)-Ho(1)-O(7)	107.17(17)	O(1)-Ho(1)-O(4)#1	164.74(16)	N(4)#3-Zn(1)-N(1)	99.60(18)
O(5)-Ho(1)-O(7)	76.86(14)	O(5)-Ho(1)-O(4)#1	95.22(14)	N(3)#2-Zn(1)-O(2)	89.49(17)
O(1)-Ho(1)-O(2w)	82.44(17)	O(7)-Ho(1)-O(4)#1	84.50(15)	N(4)#3-Zn(1)-O(2)	160.73(17)
O(5)-Ho(1)-O(2w)	136.09(15)	O(2w)-Ho(1)-O(4)#1	93.08(15)	N(1)-Zn(1)-O(2)	76.67(16)
O(7)-Ho(1)-O(2w)	146.95(14)	O(1w)-Ho(1)-O(4)#1	76.54(15)	N(3)#2-Zn(1)-O(6)#2	77.79(16)
O(1)-Ho(1)-O(1w)	88.21(17)	O(3)-Ho(1)-O(4)#1	116.94(12)	N(4)#3-Zn(1)-O(6)#2	100.65(16)
O(5)-Ho(1)-O(1w)	68.35(14)	O(1)-Ho(1)-O(3)#1	139.11(14)	N(1)-Zn(1)-O(6)#2	93.33(15)
O(7)-Ho(1)-O(1w)	138.20(15)	O(5)-Ho(1)-O(3)#1	139.61(14)	O(2)-Zn(1)-O(6)#2	98.46(16)
O(2w)-Ho(1)-O(1w)	71.92(14)	O(7)-Ho(1)-O(3)#1	77.01(12)	N(3)#2-Zn(1)-O(8)#3	100.82(17)

O(1)-Ho(1)-O(3)	76.31(14)	O(2w)-Ho(1)-O(3)#1	75.69(13)	N(4)#3-Zn(1)-O(8)#3	76.58(16)
O(5)-Ho(1)-O(3)	134.56(13)	O(1w)-Ho(1)-O(3)#1	116.20(13)	N(1)-Zn(1)-O(8)#3	88.76(17)
O(7)-Ho(1)-O(3)	75.42(14)	O(3)-Ho(1)-O(3)#1	65.27(13)	O(2)-Zn(1)-O(8)#3	84.40(16)
O(2w)-Ho(1)-O(3)	76.46(13)	O(4)#1-Ho(1)-O(3)	52.02(13)	O(6)#2-Zn(1)-O(8)#3	176.78(15)

Complex 3

Bond	Length	Bond	Length	Bond	Length
Er(1)-O(1)	2.210(3)	Er(1)-O(7)	2.273(3)	O(3)-Er(1)-O(3)#1	65.23(11)
Er(1)-O(3)	2.397(3)	Er(1)-O(1w)	2.393(3)	O(4)#1-Er(1)-O(3)#1	52.25(11)
Er(1)-O(3)#1	2.522(3)	Er(1)-O(2w)	2.324(3)	N(3)#2-Zn(1)-N(4)#3	96.55(15)
Er(1)-O(4)#1	2.441(3)	Zn(1)-O(2)	2.175(3)	N(3)#2-Zn(1)-N(1)	162.96(14)
Er(1)-O(5)	2.269(3)	Zn(1)-O(6)#2	2.214(3)	N(4)#3-Zn(1)-N(1)	99.54(15)
Bond	Angle	Bond	Angle	N(3)#2-Zn(1)-O(2)	89.78(13)
O(1)-Er(1)-O(5)	78.69(13)	O(2w)-Er(1)-O(3)	76.64(11)	N(4)#3-Zn(1)-O(2)	160.77(15)
O(1)-Er(1)-O(7)	107.44(14)	O(1w)-Er(1)-O(3)	146.23(11)	N(1)-Zn(1)-O(2)	76.78(13)
O(5)-Er(1)-O(7)	77.12(11)	O(1)-Er(1)-O(4)#1	164.82(12)	N(3)#2-Zn(1)-O(6)#2	77.84(13)
O(1)-Er(1)-O(2w)	82.15(14)	O(5)-Er(1)-O(4)#1	94.13(12)	N(4)#3-Zn(1)-O(6)#2	100.55(14)
O(5)-Er(1)-O(2w)	135.66(12)	O(7)-Er(1)-O(4)#1	83.59(12)	N(1)-Zn(1)-O(6)#2	93.66(13)
O(7)-Er(1)-O(2w)	147.14(12)	O(2w)-Er(1)-O(4)#1	94.20(13)	O(2)-Zn(1)-O(6)#2	98.52(14)
O(1)-Er(1)-O(1w)	88.75(14)	O(1w)-Er(1)-O(4)#1	76.15(12)	N(3)#2-Zn(1)-O(8)#3	100.77(14)
O(5)-Er(1)-O(1w)	68.72(12)	O(3)-Er(1)-O(4)#1	117.05(9)	O(3)-Er(1)-O(3)#1	65.23(11)
O(7)-Er(1)-O(1w)	138.41(12)	O(1)-Er(1)-O(3)#1	139.43(11)	O(4)#1-Er(1)-O(3)#1	52.25(11)
O(2w)-Er(1)-O(1w)	71.27(12)	O(5)-Er(1)-O(3)#1	139.07(11)	N(3)#2-Zn(1)-N(4)#3	96.55(15)
O(1)-Er(1)-O(3)	76.59(11)	O(7)-Er(1)-O(3)#1	76.53(10)	N(3)#2-Zn(1)-N(1)	162.96(14)
O(5)-Er(1)-O(3)	135.04(11)	O(2w)-Er(1)-O(3)#1	76.37(11)	N(4)#3-Zn(1)-N(1)	99.54(15)
O(7)-Er(1)-O(3)	75.35(11)	O(1w)-Er(1)-O(3)#1	115.47(11)	N(3)#2-Zn(1)-O(2)	89.78(13)

Complex 4

Bond	Length	Bond	Length	Bond	Length
Yb(1)-O(1)	2.192(3)	Yb(1)-O(2w)	2.299(3)	O(3)-Yb(1)#1	2.499(3)
Yb(1)-O(3)	2.390(3)	Zn(1)-O(2)	2.173(3)	O(4)-Yb(1)#1	2.420(3)
Yb(1)-O(3)#1	2.499(3)	Zn(1)-O(6)#2	2.221(3)	O(6)-Zn(1)#2	2.221(3)
Yb(1)-O(4)#1	2.420(3)	Zn(1)-O(8)#3	2.254(3)	O(8)-Zn(1)#4	2.254(3)
Yb(1)-O(5)	2.258(3)	Zn(1)-N(1)	2.122(3)	N(3)-Zn(1)#2	2.064(3)
Yb(1)-O(7)	2.256(3)	Zn(1)-N(3)#2	2.064(3)	N(4)-Zn(1)#4	2.079(3)
Yb(1)-O(1w)	2.376(3)	Zn(1)-N(4)#3	2.079(3)		
Bond	Angle	Bond	Angle	Bond	Angle
O(1)-Yb(1)-O(7)	106.58(12)	O(7)-Yb(1)-O(4)#1	83.86(11)	N(4)#3-Zn(1)-O(2)	161.10(13)
O(1)-Yb(1)-O(5)	78.66(12)	O(5)-Yb(1)-O(4)#1	93.02(11)	N(1)-Zn(1)-O(2)	76.72(12)
O(7)-Yb(1)-O(5)	77.45(10)	O(2w)-Yb(1)-O(4)#1	94.57(12)	N(3)#2-Zn(1)-O(6)#2	77.92(12)

O(1)-Yb(1)-O(2w)	82.87(13)	O(1w)-Yb(1)-O(4)#1	76.29(11)	N(4)#3-Zn(1)-O(6)#2	100.28(12)
O(7)-Yb(1)-O(2w)	146.74(11)	O(3)-Yb(1)-O(4)#1	117.25(9)	N(1)-Zn(1)-O(6)#2	94.02(11)
O(5)-Yb(1)-O(2w)	135.73(11)	O(1)-Yb(1)-O(3)#1	139.75(10)	O(2)-Zn(1)-O(6)#2	98.48(12)
O(1)-Yb(1)-O(1w)	88.56(12)	O(7)-Yb(1)-O(3)#1	76.91(9)	N(3)#2-Zn(1)-O(8)#3	100.61(12)
O(7)-Yb(1)-O(1w)	139.17(11)	O(5)-Yb(1)-O(3)#1	138.90(10)	N(4)#3-Zn(1)-O(8)#3	76.51(11)
O(5)-Yb(1)-O(1w)	68.53(10)	O(2w)-Yb(1)-O(3)#1	75.90(10)	N(1)-Zn(1)-O(8)#3	88.25(12)
O(2w)-Yb(1)-O(1w)	71.15(11)	O(1w)-Yb(1)-O(3)#1	115.38(10)	O(2)-Zn(1)-O(8)#3	84.81(12)
O(1)-Yb(1)-O(3)	77.02(10)	O(3)-Yb(1)-O(3)#1	65.02(10)	O(6)#2-Zn(1)-O(8)#3	176.36(11)
O(7)-Yb(1)-O(3)	75.01(10)	O(4)#1-Yb(1)-O(3)	52.73(10)	C(1)-O(1)-Yb(1)	153.8(3)
O(5)-Yb(1)-O(3)	135.85(10)	N(3)#2-Zn(1)-N(4)#3	96.54(14)	C(1)-O(2)-Zn(1)	116.7(3)
O(2w)-Yb(1)-O(3)	76.35(10)	N(3)#2-Zn(1)-N(1)	163.05(13)	C(4)-O(3)-Yb(1)	150.7(2)
O(1w)-Yb(1)-O(3)	145.80(10)	N(4)#3-Zn(1)-N(1)	99.59(14)	C(4)-O(3)-Yb(1)#1	91.9(2)
O(1)-Yb(1)-O(4)#1	164.60(11)	N(3)#2-Zn(1)-O(2)	89.62(12)	Yb(1)-O(3)-Yb(1)#1	114.98(10)

Complex 5

Bond	Length	Bond	Length	Bond	Length
Tb(1)-O(1)	2.241(5)	Co(1)-O(6)#3	2.162(5)	Tb(1)-O(4)#1	2.474(4)
Tb(1)-O(5)	2.288(5)	Co(1)-O(8)#2	2.178(5)	Tb(1)-O(3)#1	2.557(4)
Tb(1)-O(7)	2.298(5)	O(4)-Tb(1)#1	2.474(4)	Co(1)-N(4)#2	2.081(5)
Tb(1)-O(2W)	2.361(5)	O(6)-Co(1)#3	2.162(5)	Co(1)-N(3)#3	2.081(5)
Tb(1)-O(3)	2.413(5)	O(8)-Co(1)#4	2.178(5)	Co(1)-O(2)	2.111(5)
Tb(1)-O(1W)	2.418(5)	N(4)-Co(1)#4	2.081(5)	Co(1)-N(1)	2.135(6)

Bond	Angle	Bond	Angle	Bond	Angle
O(1)-Tb(1)-O(5)	78.68(19)	O(2W)-Tb(1)-O(3)#1	76.66(2)	O(1W)-Tb(1)-O(4)#1	76.51(17)
O(1)-Tb(1)-O(7)	107.6(2)	O(3)-Tb(1)-O(3)#1	65.83(2)	O(1)-Tb(1)-O(3)#1	139.20(17)
O(5)-Tb(1)-O(7)	76.96(17)	O(1W)-Tb(1)-O(3)#1	115.33(2)	O(5)-Tb(1)-O(3)#1	139.21(16)
O(1)-Tb(1)-O(3)	75.79(17)	O(4)#1-Tb(1)-O(3)#1	51.45(2)	O(7)-Tb(1)-O(3)#1	76.43(15)
O(5)-Tb(1)-O(3)	134.28(2)	N(4)#2-Co(1)-N(3)#3	94.6(2)	N(4)#2-Co(1)-O(6)#3	99.1(2)
O(7)-Tb(1)-O(3)	75.58(17)	N(4)#2-Co(1)-O(2)	163.9(2)	N(3)#3-Co(1)-O(6)#3	78.1(2)
O(2W)-Tb(1)-O(3)	76.86(16)	N(3)#3-Co(1)-O(2)	91.4(2)	O(2)-Co(1)-O(6)#3	96.73(19)
O(5)-Tb(1)-O(4)#1	95.19(17)	N(4)#2-Co(1)-N(1)	98.2(2)	O(7)-Tb(1)-O(1W)	138.22(18)
O(1)-Tb(1)-O(4)#1	165.54(2)	N(3)#3-Co(1)-N(1)	166.4(2)	O(3)-Tb(1)-O(4)#1	116.87(14)
O(6)#3-Co(1)-O(8)#2	175.58(2)	O(2)-Co(1)-N(1)	77.42(2)	O(2)-Co(1)-O(8)#2	86.49(18)
O(7)-Tb(1)-O(4)#1	83.34(17)	N(1)-Co(1)-O(6)#3	95.2(2)	N(1)-Co(1)-O(8)#2	88.4(2)
N(4)#2-Co(1)-O(8)	77.82(19)	N(3)#3-Co(1)-O(8)#2	98.8(2)	O(1W)-Tb(1)-O(4)#1	76.51(17)
O(1)-Tb(1)-O(5)	78.68(19)	O(2W)-Tb(1)-O(3)#1	76.66(2)		

Complex 6

Bond	Length	Bond	Length	Bond	Length
Dy(1)-O(1)	2.233(5)	Dy(1)-O(1w)	2.408(6)	Co(1)-N(3)#2	2.090(6)

Dy(1)-O(3)#1	2.545(5)	Dy(1)-O(2w)	2.352(5)	Co(1)-N(4)#3	2.089(6)
Dy(1)-O(3)	2.408(5)	Co(1)-O(2)	2.121(5)	O(3)-Dy(1)#1	2.545(5)
Dy(1)-O(4)#1	2.459(5)	Co(1)-O(6)#2	2.163(5)	O(4)-Dy(1)#1	2.459(5)
Dy(1)-O(5)	2.285(5)	Co(1)-O(8)#3	2.187(5)	O(6)-Co(1)#2	2.163(5)
Dy(1)-O(7)	2.292(5)	Co(1)-N(1)	2.143(6)	O(8)-Co(1)#4	2.187(5)
Bond	Angle	Bond	Angle	Bond	Angle
O(1)-Dy(1)-O(5)	78.3(2)	O(7)-Dy(1)-O(3)	75.67(18)	O(2w)-Dy(1)-O(3)#1	76.45(17)
O(1)-Dy(1)-O(7)	107.4(2)	O(2w)-Dy(1)-O(3)	76.16(17)	O(1w)-Dy(1)-O(3)#1	114.89(18)
O(5)-Dy(1)-O(7)	77.10(18)	O(1w)-Dy(1)-O(3)	145.79(17)	O(3)-Dy(1)-O(3)#1	65.48(17)
O(1)-Dy(1)-O(2w)	82.0(2)	O(1)-Dy(1)-O(4)#1	165.4(2)	O(4)#1-Dy(1)-O(3)#1	51.76(16)
O(5)-Dy(1)-O(2w)	135.81(19)	O(5)-Dy(1)-O(4)#1	94.91(19)	O(3)-Dy(1)-C(4)#1	91.16(16)
O(7)-Dy(1)-O(2w)	146.96(19)	O(7)-Dy(1)-O(4)#1	83.31(19)	N(4)#3-Co(1)-N(3)#2	93.9(2)
O(1)-Dy(1)-O(1w)	89.3(2)	O(2w)-Dy(1)-O(4)#1	94.3(2)	N(4)#3-Co(1)-O(2)	164.0(2)
O(5)-Dy(1)-O(1w)	69.41(18)	O(1w)-Dy(1)-O(4)#1	76.10(19)	N(3)#2-Co(1)-O(2)	91.7(2)
O(7)-Dy(1)-O(1w)	138.5(2)	O(3)-Dy(1)-O(4)#1	116.83(15)	N(4)#3-Co(1)-N(1)	98.7(2)
O(2w)-Dy(1)-O(1w)	71.17(19)	O(1)-Dy(1)-O(3)#1	139.42(18)	N(3)#2-Co(1)-N(1)	166.6(2)
O(1)-Dy(1)-O(3)	76.23(18)	O(5)-Dy(1)-O(3)#1	139.29(18)	O(2)-Co(1)-N(1)	77.3(2)
O(5)-Dy(1)-O(3)	134.70(17)	O(7)-Dy(1)-O(3)#1	76.38(16)	N(4)#3-Co(1)-O(6)#2	99.2(2)

Symmetry codes for Symmetry codes for **1**: #1 -x+1,y+1/2,-z+1/2 ,#2 x,-y+3/2,z-1/2, #3 -x, y+1/2,-z+1/2, #4 -x,y-1/2,-z+1/2, #5 -x+1,y-1/2,-z+1/2, #6 x,-y+3/2,z+1/2, #7 -x+1,-y+1,-z+1, #8 x,y-1, z. for **2**: #1 -x+3/2,-y+1/2,-z+1, #2 -x+1,-y,-z+1, #3 -x+3/2,y-1/2,-z+1/2 , #4 -x+3/2,y+1/2,-z+1/2. for **3**: #1 -x+1,-y,-z+1, #2 -x+1/2,y+1/2,-z+1/2, #3 x,-y,z+1/2, #4 -x+1/2,y-1/2,-z+1/2, #5 x,-y, z-1/2. for **4**: #1 -x+1,-y+1,-z+1, #2 -x+3/2,y-1/2,-z+3/2; #3 x+1/2,y-1/2, z, #4 -x+3/2,y+1/2,-z+3/2,#5 x-1/2,y+1/2, z. for **5**: #1 -x+1/2,-y+1/2,-z+1; #2 -x+1,-y+1,-z+1; #3 -x+1/2,y+1/2,-z+3/2; #4 -x+1/2,y-1/2,-z+3/2, for **6**: #1 -x+1,-y,-z+1 ,#2 -x+1/2,y+1/2,-z+1/2, #3 x,-y, z+1/2, #4 -x+1/2, y-1/2,-z+1/2, #5 x,-y,z-1/2.

Table S2 The hydrogen bond lengths (Å) and angles (°) for polymers **1- 6**

D-H...A	d(D-H)	d(H...A)	d(D...A)	<(DHA)
Complex 1				
O(1w)-H(11)...O(2)#6	0.84	1.94	2.76(1)	166
O(1w)-H(12)...O(2w)	0.84	1.92	2.70(1)	152
O(2w)-H(21)...O(6)#6	0.84	2.26	3.04(1)	155
O(2w)-H(22)...O(8)	0.84	2.09	2.86(1)	152
O(3w)-H(31)...O(4)#7	0.84	1.96	2.78(1)	167
O(3w)-H(32)...O(8)#8	0.84	2.32	2.98(2)	136
N(4)-H(4)...O(3w)	0.88	1.90	2.78(2)	172
Complex 2	S18			

O(1w)-H(11)...O(4)#5	0.84	2.16	2.853(6)	139.0
O(1w)-H(12)...O(3w)	0.84	2.23	2.712(6)	116.2
O(2w)-H(21)...O(7)#1	0.84	2.00	2.835(6)	171.9
O(2w)-H(22)...O(5w)	0.84	2.10	2.666(7)	124.3
O(3w)-H(31)...O(4w)	0.84	1.95	2.793(9)	177.9
O(3w)-H(32)...O(6w)	0.84	2.36	3.169(18)	162.3
O(4w)-H(41)...O(2)#6	0.84	1.93	2.750(10)	166.3
O(4w)-H(42)...O(1w)#6	0.84	2.40	2.979(10)	127.0
O(5w)-H(51)...O(4w)	0.84	1.92	2.745(13)	168.7
N(2)-H(2)...O(6)#7	0.88	2.26	2.843(6)	123.8
Complex 3				
O(1w)-H(11)...O(4)#5	0.84	2.16	2.849(5)	139.1
O(1w)-H(12)...O(3w)	0.84	2.24	2.698(5)	114.7
O(2w)-H(21)...O(7)#1	0.84	2.01	2.847(5)	171.8
O(2w)-H(22)...O(5w)	0.84	2.09	2.649(8)	123.7
O(3w)-H(31)...O(4w)	0.84	1.94	2.779(10)	178.9
O(3w)-H(32)...O(6w)	0.84	2.35	3.167(15)	163.2
O(4w)-H(41)...O(2)#6	0.84	1.90	2.725(11)	167.6
O(4w)-H(42)...O(1w)#6	0.84	2.41	2.999(10)	128.1
O(5w)-H(51)...O(4w)	0.84	1.85	2.681(15)	168.4
N(2)-H(2)...O(6)#7	0.88	2.27	2.845(5)	123.3
Complex 4				
O(1w)-H(11)...O(4)#5	0.84	2.19	2.864(4)	138.0
O(1w)-H(12)...O(3w)	0.84	2.23	2.696(4)	115.2
O(2w)-H(21)...O(7)#1	0.84	1.99	2.822(4)	172.9
O(2w)-H(22)...O(5w)	0.84	2.08	2.641(6)	124.0
O(3w)-H(31)...O(4w)	0.84	1.97	2.808(8)	178.1
O(3w)-H(32)...O(6w)	0.84	2.36	3.177(12)	163.2
O(4w)-H(41)...O(2)#6	0.84	1.91	2.737(9)	167.9
O(4w)-H(42)...O(1w)#6	0.84	2.38	2.960(8)	127.0
O(5w)-H(51)...O(4w)	0.84	1.89	2.723(12)	169.0
N(2)-H(2)...O(6)#7	0.88	2.27	2.848(5)	122.9
Complex 5				
O(1W)-H(11)...O(4)#5	0.84	2.12	2.803(7)	138.8
O(1W)-H(12)...O(3W)	0.84	2.23	2.699(7)	115.0
O(2W)-H(21)...O(7)#1	0.84	2.04	2.869(7)	171.4
O(2W)-H(22)...O(5W)	0.85	2.06	2.626(16)	123.7
O(3W)-H(31)...O(4W)	0.84	1.84	2.659(17)	163.4

O(3W)-H(32)...O(6W)	0.84	2.21	3.013(19)	160.0
O(4W)-H(41)...O(2)#6	0.84	1.87	2.701(18)	171.5
O(4W)-H(42)...O(1W)#6	0.84	2.48	3.170(17)	140.4
O(5W)-H(51)...O(4W)	0.84	1.43	2.25(3)	163.5
N(2)-H(2)...O(6)#7	0.88	2.33	2.858(8)	118.7
Complex 6				
O(1w)-H(11)...O(4)#5	0.84	2.13	2.821(8)	139.4
O(1w)-H(12)...O(3w)	0.84	2.22	2.681(8)	114.2
O(2w)-H(21)...O(7)#1	0.84	2.02	2.850(8)	171.7
O(3w)-H(31)...O(4w)	0.84	1.85	2.687	176.6
O(4w)-H(41)...O(2)#6	0.84	1.90	2.691(7)	156.4
O(4w)-H(42)...O(1w)#6	0.84	2.72	3.146(8)	113.5
N(2)-H(2)...O(6)#7	0.88	2.31	2.859(8)	120.7

Symmetry codes for Symmetry codes for **1**: #1 -x+1,y+1/2,-z+1/2 ,#2 x,-y+3/2,z-1/2, #3 -x, y+1/2,-z+1/2, #4 -x,y-1/2,-z+1/2, #5 -x+1,y-1/2,-z+1/2, #6 x,-y+3/2,z+1/2, #7 -x+1,-y+1,-z+1, #8 x,y-1, z. for **2**: #1 -x+3/2,-y+1/2,-z+1, #2 -x+1,-y,-z+1, #3 -x+3/2,y-1/2,-z+1/2 , #4 -x+3/2,y+1/2,-z+1/2. for **3**: #1 -x+1,-y,-z+1, #2 -x+1/2,y+1/2,-z+1/2, #3 x,-y,z+1/2, #4 -x+1/2,y-1/2,-z+1/2, #5 x,-y, z-1/2. for **4**: #1 -x+1,-y+1,-z+1, #2 -x+3/2,y-1/2,-z+3/2; #3 x+1/2,y-1/2, z, #4 -x+3/2,y+1/2,-z+3/2,#5 x-1/2,y+1/2, z. for **5**: #1 -x+1/2,-y+1/2,-z+1; #2 -x+1,-y+1,-z+1; #3 -x+1/2,y+1/2,-z+3/2; #4 -x+1/2,y-1/2,-z+3/2, for **6**: #1 -x+1,-y,-z+1 ,#2 -x+1/2,y+1/2,-z+1/2, #3 x,-y,z+1/2, #4 -x+1/2, y-1/2,-z+1/2, #5 x,-y,z-1/2.

References

1. Song, J. F.; Zhou, R. S.; Hu, T. P.; Chen, Z.; Wang, B. B. *J. Coord. Chem.*, **2010**, 63, 42014.
2. Feng, X.; Miao S. B.; Li, T. F. and Wang, L. Y. *Russ. J. Coord. Chem.*, **2011**, 37, 572.
3. Sun, Y. G.; Wu, Y. L.; Philippe, G. X.; Smet, F.; Ding, F.; Guo, M. Y.; Zhu, M. C.; Gao, E. J.; Poelman, D and Verpoort, F. *Dalton Trans*, **2010**, 39, 11383.
4. Paira, M. K., Dinda, J., Lu, T.H., et al., *Polyhedron*, **2007**, 26, 4131.